

Submitted to *The Astrophysical Journal*.

Double lenses

Giuseppe Bertin

and

Marco Lombardi¹

Scuola Normale Superiore, Piazza dei Cavalieri 7, I 56126 Pisa, Italy

ABSTRACT

The analysis of the shear induced by a single cluster, acting as a gravitational lens, on the images of a large number of background galaxies is all centered around the curl-free character of a well-known vector field that can be derived from the data; in particular, the mass reconstruction methods, currently producing many interesting astrophysical applications, are all based on this tensorial property of the induced shear. Such basic property breaks down when the source galaxies happen to be observed through two clusters at different redshifts, partially aligned along the line of sight, because an asymmetric part in the Jacobian matrix associated with the ray tracing transformation is expected, now that the incoming light rays are bent twice. In this paper we address the study of double lenses and obtain five main results. (i) First we generalize the procedure to extract the available information, contained in the observed shear field, from the case of a single lens to that of a double lens. (ii) Then we evaluate the possibility of detecting the signature of double lensing given the known properties of the distribution of clusters of galaxies. In particular, we show that a few configurations are likely to be present in the sky, for which the small effects characteristic of double lensing may already be within detection limits (i.e., we show that the signal involved is expected to be larger than what could be produced by statistical noise, which includes effects associated with the distribution of the source ellipticities and with the spread in redshift of the lensed galaxies). (iii) As a different astrophysical application, we demonstrate how the method can be used to detect the presence of a dark cluster that might happen to be partially aligned with a bright cluster studied in terms of statistical lensing; if the properties of the bright cluster are well constrained by independent diagnostics, the location and the structure

¹European Southern Observatory, Karl-Schwarzschild-Straße 2, Garching bei München, D-85748, Germany

of the dark cluster can be reconstructed. (iv) In addition, we show that the redshift distribution of the source galaxies, which in principle might also contribute to break the curl-free character of the shear field, actually produces systematic effects typically two orders of magnitude smaller than the double lensing effects we are focusing on. (v) Remarkably, a discussion of relevant contributions to the noise of the shear measurement has brought up an intrinsic limitation of weak lensing analyses, since one specific contribution, associated with the presence of a non-vanishing two-galaxy correlation function, turns out not to decrease with the density of source galaxies (and thus with the depth of the observations). In our mathematical framework, the contribution of the small asymmetry in the Jacobian matrix induced by double lensing is retained consistently up to two orders in the weak lensing asymptotic expansion. The analysis is then checked and exemplified by means of simulations.

Subject headings: cosmology: gravitational lensing — cosmology: dark matter — galaxies: clustering — galaxies: distances and redshifts

1. Introduction

The study of statistical gravitational lensing effects on large numbers of source galaxies due to intervening matter has been a subject of major and rapid progress both from the methodological and from the observational point of view (e.g., see Kaiser & Squires 1993; Luppino & Kaiser 1997; Taylor et al. 1998; Lombardi & Bertin 1998a, b, hereafter Paper I, II). This indeed offers a very promising approach to study the overall mass distribution, especially on the scale of clusters of galaxies. In fact, the most appealing aspect of this line of research is its diagnostic potential, with the possibility to measure mass distributions independently of the traditional tools that have to rely on the use of dynamical models.

The interest in this method has gained further momentum from the most recent developments of telescopes and instrumentation. Very deep images are now bringing in accurate data that allow us to analyze the shape of thousands of galaxies, with a density of nearly 200 galaxies arcmin⁻² already reached (see Hoekstra et al. 2000). The use of information from so many sources makes it possible to measure very small lensing effects, which would have been beyond expectation just a few years ago.

The work in this area is thus mostly addressing two directions. On the methodological side, the main hope is to develop mass reconstruction algorithms that are simple, flexible, and reliable, with full control of the errors involved in the procedure that goes from the shear data to the

inferred properties of the lens (see, e.g., Bartelmann et al. 1996; Seitz & Schneider 1997; Paper I; Paper II). On the side of data analysis, a variety of important issues have to be properly faced and addressed, in order to secure accurate shape measurements as free as possible from all the undesired or spurious distortions that are associated with the instrument and with the observation conditions (Kaiser, Squires, & Broadhurst 1995).

Within this general perspective, the present paper belongs to a third direction of research, i.e. the study of potentially interesting effects and phenomena, such as the lensing associated with gravity waves (Kaiser & Jaffe 1997) or cosmological applications where gravitational lensing probes the geometry of the universe (Kaiser 1998; Lombardi & Bertin 1999, Paper III; van Waerbeke, Bernardeau, & Mellier 1999). Measuring these effects, admittedly at the limits of current observations, is expected to become feasible with the advent of the next generation telescopes.

The theory of double lenses has already been subject to some progress. For example, it has been proven that multiple lenses produce an odd number of images from a pointlike source (Seitz & Schneider 1992) and that a simple theorem on the magnification of images holds (Seitz & Schneider 1994), while Crawford et al. (1986) have discussed the probability that a quasar is strongly lensed by two clusters. However, this still remains a challenging line of research that is so far largely unexplored; in particular, the problem has not been discussed, to our knowledge, in the important context of weak lensing analyses. Attracted by the new developments in deep imaging and especially in the observation of very distant clusters of galaxies, which already suggest that a chance alignment of two clusters is not to be considered an unlikely event (for example, see the case of Cl0317 + 15 noted by Molinari, Buzzoni, & Chincarini 1996, and of A1758 reported by Wang & Ulmer 1997), we found it natural to give further thought to such lens configurations.

In this paper, for the context of weak lensing, we generalize the procedure to extract the astrophysical information contained in the observed shear field from the case of a single lens to that of a double lens. We start by showing how the trace and the asymmetric part of the Jacobian matrix associated with the ray-tracing transformation can be measured (Sect. 2 and Sect. 3), once the observed ellipticities of a large number of background galaxies have been properly secured. We then consider some explicit questions that can be tackled in configurations of astrophysical interest; in particular, we formulate and address a “dark cluster problem,” corresponding to the situation where the signature of double lensing is observed at variance with the apparent absence of a second bright cluster partially aligned along the line of sight (Sect. 4). We then estimate the size of the effects involved (Sect. 5), so that we can state that, based on the known properties of the distribution of bright clusters, a few configurations are likely to be present in the sky, for which the small effects characteristic of double lensing may already be within detection limits. Surprisingly, a discussion of the relevant contributions to the noise of the shear measurement reveals an intrinsic

limitation of weak lensing analyses. In fact, we find that the noise contribution associated with the two-galaxy cosmological correlation function does not decrease with the depth of the observation. A quantitative evaluation of this subtle effect and of its impact on mass reconstructions deserves a separate investigation and will be considered in a future paper. Some numerical tests in Sect. 6 demonstrate that the analytical framework developed is sound and bring out the existence of some curious effects (especially on the criticality condition for a double lens and on the possibility of pinpointing the location of the invisible cluster in the dark cluster problem). Then, simulations in the same section show that the redshift distribution of the source galaxies, which in principle might also contribute to break the curl-free character of the shear field, actually produces systematic effects typically two orders of magnitude smaller than the double lensing effects we are focusing on. In addition, they suggest that reasonable assumptions on the observed galaxies lead to noise levels that do not mar the possibility of detecting the double-lensing effect. Even if, at present, much of what we have obtained is barely within the limits of direct experimental confirmation, with the advent of new instrumentation (such as ACS on HST) and powerful telescopes of the next generation (such as NGST) the observational impact of analyses of the type provided here is bound to become significant.

2. Basic relations

In this section we briefly recall the lensing equations for double lenses, in the context where the lensing is produced by intervening clusters. For the purpose, we mostly follow Schneider, Ehlers, & Falco (1992), with some small differences of notation (see also Paper III). We then summarize the principles of the statistical analysis that leads to a local measurement of the gravitational shear.

2.1. Ray-tracing equation

Let us consider for the moment a single source at redshift z^s . Let $D(z_1, z_2)$ be the angular diameter distance between two aligned objects at redshift z_1 and z_2 , and $D_{ij} = D(z^{(i)}, z^{(j)})$ (with $i, j \in \{o, 1, 2, s\}$ and $0 = z^{(o)} < z^{(1)} < z^{(2)} < z^{(s)}$) the distances between two of the elements of the lens configuration, made of observer (o), two deflector planes (1 and 2), and source plane (s). We call $\theta^{(1)}$ (or simply θ) the apparent position of the source, so that $\mathbf{x}^{(1)} = D_{o1}\theta^{(1)}$ is the corresponding linear position on the first deflector plane. The light ray is traced back to angular positions $\theta^{(2)} = \mathbf{x}^{(2)}/D_{o2}$ and $\theta^{(s)} = \mathbf{x}^{(s)}/D_{os}$ referred to the second deflector and to the source (see Fig. 1). For simplicity, in the following we will use the notation θ^s for $\theta^{(s)}$. The “dynamics”

of the two lenses is contained in two deflection functions $\alpha^{(1)}$ and $\alpha^{(2)}$, such that

$$\mathbf{x}^{(2)} = D_{o2}\boldsymbol{\theta}^{(1)} - D_{12}\boldsymbol{\alpha}^{(1)}(D_{o1}\boldsymbol{\theta}^{(1)}) , \quad (1)$$

$$\mathbf{x}^{(s)} = D_{os}\boldsymbol{\theta}^{(1)} - D_{1s}\boldsymbol{\alpha}^{(1)}(D_{o1}\boldsymbol{\theta}^{(1)}) - D_{2s}\boldsymbol{\alpha}^{(2)}(D_{o2}\boldsymbol{\theta}^{(2)}) . \quad (2)$$

Thus the *ray-tracing equation* can be written as

$$\boldsymbol{\theta}^s = \boldsymbol{\theta} - \boldsymbol{\beta}^{(1)}(\boldsymbol{\theta}) - \boldsymbol{\beta}^{(2)}(\boldsymbol{\theta} - \Delta\boldsymbol{\beta}^{(1)}(\boldsymbol{\theta})) , \quad (3)$$

with ($\ell = 1, 2$)

$$\boldsymbol{\beta}^{(\ell)}(\boldsymbol{\theta}) = \frac{D_{\ell s}}{D_{os}}\boldsymbol{\alpha}^{(\ell)}(D_{o\ell}\boldsymbol{\theta}) \quad (4)$$

and

$$\Delta = \frac{D_{os}D_{12}}{D_{1s}D_{o2}} . \quad (5)$$

For given projected mass distributions of the two lenses $\Sigma^{(\ell)}$, the distances D_{ij} enter the problem through Δ and through the two critical densities, defined as

$$\Sigma_c^{(\ell)} = \begin{cases} \infty & \text{for } z \leq z^{(\ell)} , \\ \frac{c^2 D_{os}}{4\pi G D_{\ell s} D_{o\ell}} & \text{otherwise} . \end{cases} \quad (6)$$

The definition of $\Sigma_c^{(\ell)}$ for $z \leq z^{(\ell)}$ just states that foreground sources are unaffected by the lens. The functions $\boldsymbol{\beta}^{(\ell)}(\boldsymbol{\theta})$ can be expressed by suitable integrals of the two reduced densities $\kappa^{(\ell)} = \Sigma^{(\ell)} / \Sigma_c^{(\ell)}$. For cases of interest, Δ is smaller than unity. Note that, much like in the case of a single lens, since distances enter only through the ratios D_{1s}/D_{os} and D_{2s}/D_{os} , for a family of very distant sources the ray-tracing equation (3) can be applied without explicit reference to the distance of each source, and Δ remains finite.

If the sources are located at different redshifts but not all of them are at large distance, we can still retain a form similar to Eq. (3) for the ray-tracing equation provided we introduce the appropriate *cosmological weight functions*:

$$w^{(\ell)}(z) = \frac{\Sigma_c^{(\ell)}(z^s)}{\Sigma_c^{(\ell)}(z)} . \quad (7)$$

The functions $w^{(\ell)}(z)$ give the strength of the lens ℓ on a source at redshift z relative to a source at redshift z^s . [Note that in Paper III we used a similar definition of cosmological weight function,

but took the “reference” redshift z^s at infinity. Here we prefer to avoid the limit $z^s \rightarrow \infty$.] With this definition, Eq. (3) can be rewritten as

$$\boldsymbol{\theta}^s = \boldsymbol{\theta} - w^{(1)}\boldsymbol{\beta}^{(1)}(\boldsymbol{\theta}) - w^{(2)}\boldsymbol{\beta}^{(2)}(\boldsymbol{\theta} - \Delta\boldsymbol{\beta}^{(1)}(\boldsymbol{\theta})) . \quad (8)$$

An important qualitative aspect of the two-lens ray-tracing equation is the following. In the limit where $\Delta \rightarrow 0$, the ray-tracing equation adds two contributions, $\boldsymbol{\beta}^{(1)}(\boldsymbol{\theta})$ and $\boldsymbol{\beta}^{(2)}(\boldsymbol{\theta})$, each deriving from a potential, so that the related Jacobian matrix $A = \partial\boldsymbol{\theta}^s/\partial\boldsymbol{\theta}$ is symmetric. In turn, when $\Delta \neq 0$, the Jacobian matrix is no longer guaranteed to be symmetric (in fact, the product of two symmetric matrices is not necessarily symmetric). The limit $\Delta \rightarrow 0$ occurs when the two deflectors are very close to each other.

In the *weak lensing limit* the Jacobian matrix is considered to be close to the identity matrix, $A = \text{Id} + \mathcal{O}(\epsilon)$, with the parameter ϵ measuring the strength of the lens. Equation (8) readily shows that for two lenses of comparable strength one expects a very small asymmetry in the Jacobian matrix, with $A_{12} - A_{21} = \mathcal{O}(\Delta\epsilon^2)$. In the following we will find that, in spite of the smallness of the effect involved, a weak lensing analysis, carried out to second order, can provide interesting indications as to the possibility of detecting, in realistic cases, the presence of a double lens through its signature of an asymmetry in the Jacobian matrix. Simulations will show that such indications are further encouraged when the lenses involved are relatively strong.

2.2. Local statistical analysis

Consider a large number N of extended sources all subject to the *same* Jacobian matrix A for the relevant ray-tracing. In general, as noted above, $A \neq A^T$. Let Q_{ij} be the measured quadrupole moments of the individual galaxies. These observed quantities are related to the source (unlensed) quadrupole moments Q_{ij}^s by the equation (see Schneider, Ehlers, & Falco 1992; see also Paper I)

$$Q^s = AQA^T . \quad (9)$$

In the limit $N \rightarrow \infty$, the mean value of the source quadrupoles for an isotropic population of source galaxies should be proportional to the identity matrix

$$\langle Q^s \rangle = M \text{Id} , \quad (10)$$

with M a positive constant. This is the starting point of the Q -method described in Paper I and allows us to invert the relation for the mean values

$$A\langle Q \rangle A^T = \langle Q^s \rangle = M \text{Id} , \quad (11)$$

into

$$AA^T = M(\langle Q \rangle)^{-1} . \quad (12)$$

Note that the matrix (AA^T) is symmetric. Here we have taken $\langle Q \rangle$ to be non-singular.

The process of mass reconstruction makes use of the departures from the identity matrix of the ray tracing matrix as brought out by the observed quadrupoles. In practice, the true Jacobian matrix A_0 is considered to be unknown. Equation (12) shows that if A_0 is a solution, any matrix $A = UA_0$ obtained by multiplication by an orthogonal matrix (so that $UU^T = \text{Id}$) is also a solution. Thus in the determination of the shear associated with gravitational lensing the Jacobian matrix is bound to be identified only up to an orthogonal matrix. It is easy to show that any solution A for a problem for which A_0 is a solution can be written as $A = UA_0$, with U a suitable orthogonal matrix.

The same set of data $\{Q^{(n)}\}$ can be analyzed by a standard single lens procedure, leading to the determination of a symmetric Jacobian matrix A_s , with the property $A_s = A_s^T$. Then A_s is to be related to the true Jacobian matrix A_0 by means of an orthogonal matrix. In fact, for a given A_0 , there are in general four different symmetric matrices available (corresponding to matrices that differ by the sign of their eigenvalues). If we restrict the attention to transformations with positive determinant (the $\det U = \pm 1$ ambiguity reflects the well-known $g \mapsto 1/g^*$ invariance; see Schneider & Seitz 1995), we can write

$$A_s = \begin{pmatrix} \cos \tau & \sin \tau \\ -\sin \tau & \cos \tau \end{pmatrix} A_0 , \quad (13)$$

with

$$\tan \tau = -\frac{\varepsilon_{kk'} A_{0kk'}}{A_{0mm}} . \quad (14)$$

Here ε_{ij} is the totally antisymmetric tensor of rank 2 and $A_{0kk} = \text{Tr}(A_0)$ is the trace of A_0 (we use the summation convention on repeated indices). Note that the quantity $\varepsilon_{kk'} A_{0kk'} = A_{012} - A_{021}$ is a measure of the asymmetry of A_0 .

The symmetric matrix can thus be given in explicit form:

$$A_{sij} = \pm \frac{1}{f} (A_{0ij} A_{0mm} + \varepsilon_{jj'} A_{0ij'} \varepsilon_{kk'} A_{0kk'}) , \quad (15)$$

with

$$f^2 = (A_{0mm})^2 + (\varepsilon_{kk'} A_{0kk'})^2 . \quad (16)$$

In what has been described so far, A is considered to be the same for all the source galaxies. Therefore at this stage we have addressed only the problem of a *local* analysis, applicable to source galaxies very close to each other, in a small patch of the sky, and at a similar redshift. In conclusion, we have so far shown that a local measurement cannot lead to discovering a double lens, because there is always a way to interpret the data by means of a symmetric ray-tracing Jacobian matrix.

3. Non-local analysis in the weak lensing limit

Let us first consider only sources located at a given redshift z . In the weak lensing limit, the Jacobian matrix for such sources is of the form $A_0 = \text{Id} + \mathcal{O}(\epsilon)$, and the asymmetry is small, $\varepsilon_{kk'} A_{0kk'} = \mathcal{O}(\epsilon^2)$. Thus we can write the related symmetric matrix (the “effective” Jacobian matrix) as

$$A_s = \begin{pmatrix} \sigma + \gamma_1 & \gamma_2 \\ \gamma_2 & \sigma - \gamma_1 \end{pmatrix} \simeq \begin{pmatrix} A_{011} & A_{012} + \tau \\ A_{021} - \tau & A_{022} \end{pmatrix} \quad (17)$$

with (see Eq. (14))

$$\tau \simeq -\frac{1}{2}(A_{012} - A_{021}) = \mathcal{O}(\epsilon^2) . \quad (18)$$

Therefore the elements of the symmetric matrix (appearing in the mass reconstruction analysis) can be expressed in terms of those of the true Jacobian matrix, as

$$\sigma = \frac{1}{2} \text{Tr}(A_0) , \quad (19)$$

$$\gamma_1 = \frac{1}{2}(A_{011} - A_{022}) , \quad (20)$$

$$\gamma_2 = \frac{1}{2}(A_{012} + A_{021}) . \quad (21)$$

From inspection of Eqs. (18) and (19) and from the definition of the *true* Jacobian matrix, we find that the *true* source positions are related to σ and to τ by

$$\nabla \cdot \boldsymbol{\theta}^s = \text{Tr}(A_0) = 2\sigma , \quad (22)$$

$$\nabla \wedge \boldsymbol{\theta}^s = -(A_{012} - A_{021}) = 2\tau . \quad (23)$$

Thus, if we refer to the vector field $\mathbf{u}(\boldsymbol{\theta})$ commonly used in weak lensing analyses, we find

$$\mathbf{u} = - \begin{pmatrix} \gamma_{1,1} + \gamma_{2,2} \\ \gamma_{2,1} - \gamma_{1,2} \end{pmatrix} = -\frac{1}{2} \nabla^2 \boldsymbol{\theta}^s . \quad (24)$$

If we now combine the definition of $\mathbf{u}(\boldsymbol{\theta})$ with the above relations for σ and τ we get

$$\nabla \cdot \mathbf{u} = -\nabla^2 \sigma , \quad (25)$$

$$\nabla \wedge \mathbf{u} = -\nabla^2 \tau . \quad (26)$$

The last two equations replace the well-known relations applicable to single lens analyses, i.e. $\mathbf{u} = -\nabla \sigma$ and $\nabla \wedge \mathbf{u} = 0$.

Suppose now that the source galaxies follow a redshift distribution $p(z)$. At each redshift, we can apply Eqs. (17–26) provided that all lensing quantities, such as A_0 , σ , γ , and τ , are calculated for each source at the correct redshift. In the weak lensing limit, the shear γ is estimated from the ellipticities of galaxies that are observed in a particular region of the sky. Since source galaxies have different redshifts, in reality a mean value of the shear is measured:

$$\langle \gamma \rangle_z = \int_0^\infty \gamma(z) p(z) dz , \quad (27)$$

where $\gamma(z)$ is the redshift-dependent shear. In the weak lensing limit, all quantities depend linearly on the shear, and thus Eqs. (25) and (26) can be written as

$$\nabla \cdot \langle \mathbf{u} \rangle_z = -\nabla^2 \langle \sigma \rangle_z , \quad (28)$$

$$\nabla \wedge \langle \mathbf{u} \rangle_z = -\nabla^2 \langle \tau \rangle_z . \quad (29)$$

Unfortunately, these relations cannot be used to infer directly, from a given set of data, the amount of asymmetry that would be a characteristic signature of multiple lensing. The reason is that for this purpose the data should be able to identify the vector field $\mathbf{u}(\boldsymbol{\theta})$ up to $\mathcal{O}(\epsilon^2)$, because we know that $\tau = \mathcal{O}(\epsilon^2)$. In practice, it is well-known that standard weak lensing analyses lead to the determination of $\mathbf{u}(\boldsymbol{\theta})$ only up to $\mathcal{O}(\epsilon)$. In fact, observations lead to the determination of the *reduced shear* $g(\boldsymbol{\theta}) = \gamma(\boldsymbol{\theta})/\sigma(\boldsymbol{\theta})$; the identification of g with γ is correct only to $\mathcal{O}(\epsilon)$. Thus the above analysis is not yet ready for practical applications. For this reason we need to extend the discussion so as to include the *second order* terms in the weak lensing expansion. In principle, the discussion can be carried out by retaining the redshift dependence of sources. In practice, such approach would lead us far beyond the original purpose of this paper. For this reason we will suppose, in the following, that all sources are located at redshift z^s (in Sect. 5 we will consider again the spread of sources in redshift for the single lens case).

For a population of source galaxies located at a single redshift (even in the case of strong lensing; but in this section, we recall, we are still within the weak lensing expansion) an “observable” field is (see Kaiser 1995)

$$\tilde{\mathbf{u}} = \frac{1}{1 - |g|^2} \begin{pmatrix} 1 + g_1 & g_2 \\ g_2 & 1 - g_1 \end{pmatrix} \begin{pmatrix} g_{1,1} + g_{2,2} \\ g_{2,1} - g_{1,2} \end{pmatrix} ; \quad (30)$$

for a strong single lens, such field has the important property that $\tilde{\mathbf{u}} = \nabla[\ln|1 - \kappa(\boldsymbol{\theta})|]$, with $\kappa(\boldsymbol{\theta})$ the dimensionless projected density that one aims at reconstructing. Curiously, *to second order* in the weak lensing expansion (see Appendix A), it is possible to show that, for multiple weak lenses of comparable strength,

$$\nabla \cdot \tilde{\mathbf{u}} = \nabla^2(\ln \sigma) , \quad (31)$$

$$\nabla \wedge \tilde{\mathbf{u}} = \nabla^2 \tau . \quad (32)$$

In other words, *we have derived a set of equations for which the contribution of a small asymmetry present in the true Jacobian matrix is retained consistently*; the structure is similar to that of the set for $\mathbf{u}(\boldsymbol{\theta})$ field presented in Eqs. (25) and (26). *The new set of Eqs. (31) and (32) is the basis that allows us to generalize the procedure to extract the available information, contained in the observed shear field, from the case of a single lens to that of a multiple lens and thus to investigate quantitatively the characteristics of the coupling of two or more deflectors located along the same line of sight.* The symmetric limit, which we may call in this context the single lens limit, is easily recognized.

The results of this section (Eqs. (31) and (32)) are not generalized easily to the case of sources distributed according to a $p(z)$. However, the simulations described in Sect. 6.2 will basically support a description analogous to that given by Eqs. (28) and (29).

The conclusions of this section, that the data contained in the *shear map* can be used to detect an asymmetry in the true Jacobian matrix A_0 , and of the previous Sect. 2.2, that such a detection is impossible if based on a local measurement only, do not depend on the number of deflectors involved in a multiple lens. In the following, we will specialize our conclusions to the study of double lenses, for which the ray-tracing equation can be handled in a straightforward manner.

4. Double lenses in the astrophysical context

In this section we formulate some questions that may be interesting from the astrophysical point of view. The expected size of some effects and the possibility of an actual measurement will be addressed in separate sections at the end of the paper.

4.1. Where to look for the signature of double lensing?

The prime signature of double lensing would be the detection of a significant asymmetry τ (see Eq. (32)). Because of statistical errors, the measured vector field $\tilde{\mathbf{u}}$ is bound to be associated

with a non-vanishing curl. Therefore, a positive detection of asymmetry can be claimed only if the expected statistical error on τ is smaller than the true value τ_0 characterizing the double lens.

A quantitative analysis of this condition will be provided in Sect. 5 below. Here we only note that, in general, for two clusters of comparable strength, at different distances, with offset centers with respect to the line of sight, the regions on the sky where the signal-to-noise ratio for τ should be largest are those, on either side, just off the line connecting the cluster centers (see Fig. 3 and Fig. 14)

As we have seen in Sect. 2, the asymmetry is expected to be weak ($\mathcal{O}(\Delta\epsilon^2)$) for two clusters of comparable strength ϵ). The optimal conditions for detecting double lensing are then:

- The geometric parameter Δ should be close to unity, i.e., for a given distribution of sources, the distance between the two clusters should not be much smaller than the distance from the observer to the near cluster. This condition is reasonably satisfied if, for example, the redshifts of the two clusters are in the following relation, $z^{(2)} \simeq 4z^{(1)}$.
- The two clusters should be not too weak. It is preferable to consider cases where the dimensionless densities, $\kappa^{(1)}$ and $\kappa^{(2)}$, are of order unity.
- The cluster centers should be offset, but there should be a region of significant overlap between the two clusters in the sky.

4.2. Probability of cluster alignments

Given the above criteria, we now estimate the probability that a double lens with desired properties be observed. For the purpose, we refer to $H_0 = 65 \text{ km s}^{-1} \text{ Mpc}^{-1}$ for the Hubble constant, within a Friedmann-Lemaître cosmological model characterized by $\Omega = 0.3$ and $\Omega_\Lambda = 0.7$.

First, we suppose that a nearby cluster is observed at redshift $z^{(1)} \approx 0.1$ (the values of the various quantities used here are similar to the values used in the simulations to be described in Sect. 6) and ask what is the probability of finding a cluster at redshift $z^{(2)} \approx 4z^{(1)}$ well aligned with the first cluster; in considering this question, we further require that the second cluster be sufficiently massive, with mass greater than $5 \times 10^{14} \text{ M}_\odot$. For the purpose, we assume that the angular distance between the centers of the two clusters be between 2 and 4 arcmin and that the redshift of the second cluster be in the range $0.3 \leq z^{(2)} \leq 0.5$. A simple calculation then shows that the center of the second cluster must be inside a comoving volume with size $V \approx 10\,360 \text{ Mpc}^3$. Therefore, based on the cluster density found by Borgani et al. (1999; see

also Girardi et al. 1998), the expected probability of finding a “good” double lens turns out to be $\approx 0.3\%$. If we consider less strict requirements, with an angular distance between the two cluster centers in the range 1–5 arcmin and a redshift range 0.2–0.6 for the second cluster, the estimated probability increases up to $\approx 1\%$.

These estimates should be combined with the number of massive clusters at small redshift (for the object observed at $z^{(1)}$) that should be available over the whole sky. The comoving volume for a shell with redshift between 0.05 and 0.15 is $\approx 1.34 \times 10^9 \text{ Mpc}^3$; correspondingly, the total number of clusters with mass above $5 \times 10^{14} \text{ M}_\odot$ in such a volume is about 350. As a result, we expect from 1 to 3 cases of double lenses with detectable effects and configurations similar to the one considered in our simulations. From the way we have approached the problem, it is clear that the estimate just obtained provides only a *lower limit* with respect to the number of good cases expected for the purposes of the present paper.

4.3. Mass reconstruction for double lenses

Suppose that a set of data leads to the determination of $\tilde{\mathbf{u}}$ and that, based on suitable boundary conditions (e.g., $\tau(\boldsymbol{\theta}) \rightarrow 0$, $\sigma(\boldsymbol{\theta}) \rightarrow 1$ for $\|\boldsymbol{\theta}\| \rightarrow \infty$), we integrate Eqs. (31) and (32) and get the functions $\sigma(\boldsymbol{\theta})$ and $\tau(\boldsymbol{\theta})$. For a single lens problem the lensing analysis, at this stage, would be complete, since we would have the dimensionless projected mass distribution $\kappa(\boldsymbol{\theta}) = 1 - \sigma(\boldsymbol{\theta})$ associated with the deflector; knowledge of the critical density Σ_c would lead to the projected mass distribution $\Sigma(\boldsymbol{\theta})$. In the case of a double lens, what would be the astrophysically interesting quantities that could be derived?

For the following discussion, the ray-tracing equation can be re-cast in a more transparent form in the case $z = z^{(s)}$ (so that $w^{(1)} = w^{(2)} = 1$). If we introduce the two *curl-free lensing maps* (we recall that $\nabla \wedge \boldsymbol{\beta}^{(\ell)} = 0$)

$$\boldsymbol{\zeta}^{(1)}(\boldsymbol{\theta}) = \boldsymbol{\theta} - \Delta \boldsymbol{\beta}^{(1)}(\boldsymbol{\theta}) , \quad (33)$$

$$\boldsymbol{\zeta}^{(2)}(\boldsymbol{\theta}) = \boldsymbol{\theta} - \Delta \boldsymbol{\beta}^{(2)}(\boldsymbol{\theta}) , \quad (34)$$

and the *effective ray-tracing map*

$$\boldsymbol{\zeta}^s(\boldsymbol{\theta}) = (1 - \Delta)\boldsymbol{\theta} + \Delta \boldsymbol{\theta}^s(\boldsymbol{\theta}) , \quad (35)$$

we see that Eq. (8) can be written as

$$\boldsymbol{\zeta}^s(\boldsymbol{\theta}) = \boldsymbol{\zeta}^{(2)}(\boldsymbol{\zeta}^{(1)}(\boldsymbol{\theta})) . \quad (36)$$

In other words, ray-tracing for a double lens can be seen as the composition of two curl-free functions.

The double lens problem in its *direct* formulation involves two (dimensionless) ray-tracing functions ($\beta^{(1)}(\theta)$ and $\beta^{(2)}(\theta)$), two critical densities ($\Sigma_c^{(1)}$ and $\Sigma_c^{(2)}$), and one additional geometric parameter Δ . Any inverse problem would be under-determined, if we start from the two dimensionless functions $\sigma(\theta)$ and $\tau(\theta)$ alone. Even if the geometry is taken to be known (for example, when the distances to the two clusters acting as deflectors are known), it is not possible from the pair (σ, τ) to “reconstruct the two lenses,” i.e. to get the ray-tracing functions $\beta^{(1)}$ and $\beta^{(2)}$ separately. This statement is easy to understand, especially if we refer to the curl-free lensing maps $\zeta^{(1)}$ and $\zeta^{(2)}$ of Sect. 2.1. In fact, a simple scaling invariance $\zeta^{(1)} \mapsto k\zeta^{(1)}$, $\zeta^{(2)} \mapsto k^{-1}\zeta^{(2)}$ shows that, unless we are able to provide suitable boundary conditions on the functions $\zeta^{(\ell)}(\theta)$ (e.g., $\zeta^{(2)}(\theta) \rightarrow 1$ for large $\|\theta\|$), there is no way to disentangle from the shear data alone the contributions of the two lenses. Obviously, this does not mean that the lensing analysis is useless; it is only a reminder that in this more complex situation an unambiguous mass reconstruction based on weak lensing would require additional input from other probes of mass distributions (e.g., X-ray data).

In order to clarify this point further, it may be instructive to consider the following simple examples, all characterized by $\tau = 0$.

4.3.1. Aligned, centrally symmetric lenses

Suppose that

$$\zeta^s(\theta) = \frac{\theta}{\|\theta\|} \zeta^s(\|\theta\|) , \quad (37)$$

with $\zeta^s(\theta)$ a real continuous function such that $\zeta^s(0) = 0$. Then it is natural to choose $\zeta^{(1)}$ and $\zeta^{(2)}$ to be radial, i.e.

$$\zeta^{(1)}(\theta) = \frac{\theta}{\|\theta\|} \zeta^{(1)}(\|\theta\|) , \quad (38)$$

$$\zeta^{(2)}(\theta) = \frac{\theta}{\|\theta\|} \zeta^{(2)}(\|\theta\|) , \quad (39)$$

where $\zeta^{(1)}$ and $\zeta^{(2)}$ are real functions. Supposing that $\zeta^{(1)}(\theta) \geq 0$ for all θ , we can rewrite Eq. (36) as

$$\zeta^{(2)}(\zeta^{(1)}(\theta)) = \zeta^s(\theta) . \quad (40)$$

Thus reduced to a one-dimensional problem, it is clear that this equation in general admits an infinite number of solutions.

4.3.2. The general case of double lenses without asymmetry ($\tau = 0$)

Consider an effective ray-tracing map (see Eq. (35)) such that $\nabla \wedge \zeta^s = \nabla \wedge \theta^s = 0$. In this case we can solve Eq. (36) by choosing an invertible curl-free map $\zeta^{(2)}$ and by writing

$$\zeta^{(1)}(\theta) = (\zeta^{(2)})^{-1}(\zeta^s(\theta)) . \quad (41)$$

We now require that $\zeta^{(1)}$ be curl-free. From the above equation, this happens if and only if the product of the Jacobian matrix $A^{(-2)}$, associated with $(\zeta^{(2)})^{-1}$, and A^s , associated with ζ^s , is a symmetric matrix, i.e.

$$A^{(-2)}A^s = (A^{(-2)}A^s)^T = A^sA^{(-2)} . \quad (42)$$

From linear algebra we know that this is equivalent to saying that $A^{(-2)}$ and A^s have the same eigenvectors. Since $\zeta^{(2)}$ is curl-free, let us introduce the potential $\phi^{(2)}$ so that $\zeta^{(2)} = \nabla\phi^{(2)}$ and $A_{ij}^{(2)} = \phi_{,ij}^{(2)}$. If $\xi = (\xi_1, \xi_2)$ is a *local* system of coordinates where A^s is diagonal, then Eq. (42) is satisfied if $A^{(2)}$ is diagonal in the same system of coordinates, i.e. if $\partial^2\phi^{(2)} / \partial\xi_1\partial\xi_2 = 0$. This simply states that $\phi^{(2)}$ is *separable* in ξ_1 and ξ_2 , i.e. that we can write $\phi^{(2)}$ as the sum of an arbitrary function of ξ_1 and of an arbitrary function of ξ_2 . This again demonstrates the freedom at our disposal in solving Eq. (36). In addition, one can now better appreciate why, even when natural boundary conditions are specified, in general there is no guarantee that the solution be determined uniquely; in fact, several solutions are expected when the coordinate system (ξ_1, ξ_2) is associated with *poles* (such as the point $r = 0$ for polar coordinates).

4.3.3. Two lenses with no net lensing?

One curious case that may be imagined is the possibility of combining two lenses with no net effect, so that $\zeta^s(\theta) = \theta$ (see Eq. (35)). In principle, one may argue that from any invertible curl-free map $\zeta^{(1)}(\theta)$ one can take a second lens characterized by $\zeta^{(2)}(\theta) = (\zeta^{(1)}(\theta))^{-1}$. This idea would obviously generate an infinite number of solutions since the starting function $\zeta^{(1)}$ is at our disposal. However, if we require that the density distributions associated with the two lenses be both *positive definite*, i.e. that $\nabla \cdot \zeta^{(i)} \leq 2$, it can be shown that there is no way for two lenses to exactly compensate for each other: in other words, the only admissible solution is the trivial $\zeta^{(1)}(\theta) = \zeta^{(2)}(\theta) = \theta$. This conclusion is consistent with the theorem that states that any combination of gravitational lenses is bound to produce a net magnification ($\mu > 1$; see Seitz & Schneider 1992).

4.4. The dark cluster problem

A different problem based on double lenses can be formulated in the following way. Suppose that one observes a lensing cluster and that in the process of producing the mass reconstruction one finds evidence that the vector field $\tilde{\mathbf{u}}$ is not curl-free, well above the expected errors. Clearly, in such a situation, one possibility is that a separate mass concentration, which we may call a *dark cluster*, is responsible for the effect. We may now consider the case when the mass distribution of the visible cluster is well constrained by diagnostics independent of lensing (e.g., by X-ray data). Under these circumstances, what can we tell about the dark cluster properties from the observed lensing effects? In particular, is it possible to derive the location and the mass distribution of the invoked dark cluster?

If the mass distribution of the luminous cluster is taken to be known, one has either the function $\zeta_{\Delta}^{(1)}$ or the function $\zeta_{\Delta}^{(2)}$, depending on whether the dark cluster is near or far; in either case, the deflection associated with the dark cluster $\beta^{(d)} = (\boldsymbol{\theta} - \zeta^{(d)})/\Delta$ depends implicitly (see Eqs. (33)–(35)) on the geometric parameter Δ , which is unknown. One way to obtain the value of Δ is to impose that the lensing map associated with the dark cluster is curl-free, i.e. that either

$$\nabla \wedge \left[\zeta_{\Delta}^s ((\zeta_{\Delta}^{(1)})^{-1}(\boldsymbol{\theta})) \right] = 0 , \quad (43)$$

or that

$$\nabla \wedge \left[\zeta_{\Delta}^{(2)} ((\zeta_{\Delta}^s)^{-1}(\boldsymbol{\theta})) \right] = 0 , \quad (44)$$

depending on whether we guess the dark cluster to be near or far. In Sect. 6 below, by means of a simulated case, we will show how Δ can be determined with reasonable accuracy, by minimizing the square of the left side of the above equations. In other words, under the above circumstances *we will demonstrate that a weak lensing analysis allows us to pinpoint the location of the invisible cluster and to reconstruct its mass distribution.*

In closing this section, we may note that the problem of a *single* dark cluster, i.e. the case of a matter concentration detected by lensing effects without a visible counterpart for the lens, is less constrained and, in this respect, less interesting than the case discussed above in the sense that the usual mass reconstruction would only lead to the dimensionless projected density κ , with no hope to derive the distance to the dark cluster that is invoked and the actual scale of the mass involved.

5. Size of the double lensing effect

In this section we calculate the expected order of magnitude for the measurable effects associated with double lensing. For simplicity, the following section discusses the noise properties

of quantities related to the vector \mathbf{u} . The results obtained are the leading order estimates for the desired quantities related to $\tilde{\mathbf{u}}$. The following subsection deals with a population of source galaxies located at a single redshift. Effects related to a spread in redshift will be estimated in Sect. 5.3.

5.1. Expected variance of $\nabla \wedge \mathbf{u}$ for a single lens

Consider a single lens, characterized by true Jacobian matrix A_0 , so that the shear field \mathbf{u}_0 has vanishing curl, i.e. $\tau_0 = 0$. Because of the finite number of source galaxies used and of the smoothing introduced in the reconstruction process, we expect that the measured \mathbf{u} in general differs from the true field \mathbf{u}_0 .

In order to calculate the expectation value and the variance of $\nabla \wedge \mathbf{u}$, we may use a technique similar to that described in Paper II. We first recall that in the reconstruction process Eq. (12) is used together with a (positive) weight function $W(\boldsymbol{\theta}, \boldsymbol{\theta}')$. Such weight function, defined so that $W(\boldsymbol{\theta}, \boldsymbol{\theta}')$ is significantly different from zero only for $\boldsymbol{\theta}'$ close to $\boldsymbol{\theta}$, enters in the local averages of quadrupoles (or ellipticities). In particular, if we resort to the so-called Q-method associated with Eq. (12) (see Paper I), the local average quadrupole $\langle Q \rangle(\boldsymbol{\theta})$ is calculated from the relation

$$\langle Q \rangle(\boldsymbol{\theta}) = \frac{\sum_n W(\boldsymbol{\theta}, \boldsymbol{\theta}^{(n)}) Q^{(n)}}{\sum_n W(\boldsymbol{\theta}, \boldsymbol{\theta}^{(n)})} . \quad (45)$$

Here the superscripts (n) label the galaxies affected by lensing. In Paper II we have calculated expectation values and variances of several quantities, under the hypothesis that the weight function is invariant upon translation, so that $W(\boldsymbol{\theta}, \boldsymbol{\theta}') = W(\boldsymbol{\theta} - \boldsymbol{\theta}')$, and that it is *normalized*, i.e.

$$\rho \int W(\boldsymbol{\theta}) d^2\theta = 1 . \quad (46)$$

Here ρ is the density of galaxies (taken to be constant over the field). In particular, we have shown that the expectation values of the relevant quantities (in particular, the measured shear, the field \mathbf{u} , and the reconstructed mass density κ) are equal to the true quantities *smoothed* by the weight function, e.g.

$$\langle \mathbf{u} \rangle(\boldsymbol{\theta}) = \rho \int W(\boldsymbol{\theta} - \boldsymbol{\theta}') \mathbf{u}_0(\boldsymbol{\theta}') d^2\theta' . \quad (47)$$

From this expression it can be easily shown that the expected value for the measured curl of \mathbf{u}

vanishes. In fact,

$$\begin{aligned}\langle \nabla \wedge \mathbf{u} \rangle(\boldsymbol{\theta}) &= \rho \nabla_{\boldsymbol{\theta}} \wedge \int W(\boldsymbol{\theta} - \boldsymbol{\theta}') \mathbf{u}_0(\boldsymbol{\theta}') d^2\theta' \\ &= \rho \int W(\boldsymbol{\theta}') \nabla_{\boldsymbol{\theta}} \wedge \mathbf{u}_0(\boldsymbol{\theta} - \boldsymbol{\theta}') d^2\theta' = 0 .\end{aligned}\tag{48}$$

Here we have used the symmetry property of convolutions. Thus, for a single lens, we expect to measure (in the average) a field \mathbf{u} with vanishing curl. Note that, for a double lens, a similar calculation would show that

$$\langle \tau \rangle(\boldsymbol{\theta}) = \rho \int W(\boldsymbol{\theta} - \boldsymbol{\theta}') \tau_0(\boldsymbol{\theta}') d^2\theta' .\tag{49}$$

Let us now turn to covariances. Using the same notation as in Paper III (see also Lombardi 2000), we call c the covariance of the ellipticity distribution for the population of source galaxies ($\langle \epsilon_i^s \epsilon_j^s \rangle = c \delta_{ij}$). There we have shown that the covariance of the shear γ is

$$\begin{aligned}\text{Cov}_{ij}(\gamma; \boldsymbol{\theta}, \boldsymbol{\theta}') &\equiv \langle (\gamma_i(\boldsymbol{\theta}) - \langle \gamma_i \rangle(\boldsymbol{\theta})) (\gamma_j(\boldsymbol{\theta}') - \langle \gamma_j \rangle(\boldsymbol{\theta}')) \rangle \\ &= c \rho \delta_{ij} \int W(\boldsymbol{\theta} - \boldsymbol{\theta}'') W(\boldsymbol{\theta}' - \boldsymbol{\theta}'') d^2\theta'' .\end{aligned}\tag{50}$$

Note that the covariance of γ , which we may write in short as $\text{Cov}(\gamma)$, depends only on $\boldsymbol{\theta} - \boldsymbol{\theta}'$. Then the covariance of \mathbf{u} is related to the covariance of γ in a simple way:

$$\text{Cov}(\mathbf{u}) = -\nabla^2 \text{Cov}(\gamma) .\tag{51}$$

Similarly, it can be shown that

$$\text{Cov}(\nabla \wedge \mathbf{u}) = -\nabla^2 \text{Cov}(\mathbf{u}) = \nabla^2 \nabla^2 \text{Cov}(\gamma) .\tag{52}$$

The last expression is the basis of the following discussion. In fact, we may argue that a lens can be considered to be double only if the measured value of $\nabla \wedge \mathbf{u}$ is significantly larger than the expected error on this quantity. If we refer to Eqs. (18), (19) as definitions of σ and τ , we thus find (under optimal conditions defined in Paper II)

$$\text{Cov}(\sigma) = \text{Cov}(\tau) = \text{Cov}(\gamma) .\tag{53}$$

A more useful expression can be found in the simple case of a Gaussian weight function:

$$W(\boldsymbol{\theta}, \boldsymbol{\theta}') = \frac{1}{2\pi\rho\sigma_W^2} \exp\left(-\frac{\|\boldsymbol{\theta} - \boldsymbol{\theta}'\|^2}{2\sigma_W^2}\right) .\tag{54}$$

In this case we have

$$\text{Cov}_{ij}(\gamma; \boldsymbol{\delta}) = \frac{c\delta_{ij}}{4\pi\rho\sigma_W^2} \exp\left(-\frac{\|\boldsymbol{\delta}\|^2}{2\sigma_W^2}\right), \quad (55)$$

$$\begin{aligned} \text{Cov}(\nabla \wedge \mathbf{u}; \boldsymbol{\delta}) &= \frac{c \left[(8\sigma_W^2 - \|\boldsymbol{\delta}\|^2)^2 - 32\sigma_W^4 \right]}{64\pi\rho\sigma_W^{10}} \times \\ &\times \exp\left(-\frac{\|\boldsymbol{\delta}\|^2}{2\sigma_W^2}\right), \end{aligned} \quad (56)$$

where we have called $\boldsymbol{\delta} \equiv \boldsymbol{\theta} - \boldsymbol{\theta}'$. Note that $\nabla \wedge \mathbf{u}$ shows anti-correlation for $\|\boldsymbol{\delta}\|$ in the range $(2\sqrt{2} - \sqrt{2}, 2\sqrt{2} + \sqrt{2})\sigma_W$. Similar noise properties are associated with the quantity $\nabla \cdot \mathbf{u}$.

5.2. Condition for the detection of double lensing

Now we are finally able to set a quantitative condition for the detection of double lensing. The requirement that the error on τ (which can be estimated from Eqs. (53) and (55)) be smaller than the expected value of τ , within factors of order unity, can be written as:

$$\Delta\kappa^{(1)}\kappa^{(2)} \gtrsim \sqrt{\frac{c}{\rho\sigma_W^2}}. \quad (57)$$

Note that $\rho\sigma_W^2$ represents the number of galaxies effectively used in the average of Eq. (45). If we refer to a case with $\kappa^{(1)} \simeq \kappa^{(2)} \simeq \Delta \simeq 1/2$ and to the currently “realistic” density $\rho \simeq 100 \text{ gal arcmin}^{-2}$, with $c \simeq 0.03$, we thus find that a significant signal requires the use of a Gaussian weight function with smoothing size σ_W not smaller than $10''$. On the other hand, the interesting effects are those associated with the structure of the field $\tau(\boldsymbol{\theta})$, which is associated with a length scale at best comparable with that of the clusters under investigation. Therefore, we may argue that the most promising way to identify the effects of double lensing is to work with the smallest smoothing size σ_W compatible with condition (57). These arguments and the applicability of the condition defined by Eq. (57) are clarified and further supported by the simulations that will be presented in Sect. 6.

5.3. Effects related to the spread in the distances of the source galaxies

So far, in this section, we have referred to a sheet of source galaxies at a given distance. In real situations where the source galaxies are distributed at different redshifts, we expect three separate effects that can have a significant impact on our analysis:

- An extra source of noise, related to the distribution in redshift of the individual sources, is added to our data. As a result, the measured shear will have a larger covariance than the one calculated in Eq. (50), and thus a larger covariance is also expected for $\nabla \wedge \mathbf{u}$.
- An additional effect is induced by the extra-clumping of the sources described by the cosmological two-point correlation function (see Peebles 1980).
- Outside the limit of very weak lensing, there is actually no guarantee that $\nabla \wedge \tilde{\mathbf{u}} = 0$ *even in the standard case of a single lens*. This happens because the observable is, in this case, $\langle g \rangle_z$, which is not simply related to κ_0 and γ_0 .

The first two items contribute to the estimate of the relevant covariances while the third item adds a bias (to be discussed in Sect. 5.3.2).

5.3.1. Extra contributions to the covariance

Below we will estimate the covariance of the measured shear γ when the source galaxies are located at different (unknown) redshifts. For the purpose, we assume that the redshift distribution of galaxies is known. In particular, we write the probability to find one galaxy in an area $d^2\theta$ of the sky with redshift between z and $z + dz$ as

$$P_1 = \rho p(z) d^2\theta dz . \quad (58)$$

Here we model the galaxy angular distribution in terms of a constant galaxy density ρ on the lens plane. The probability to find two galaxies, one in a patch $d^2\theta^{(1)}$ of the sky with redshift in the range $[z^{(1)}, z^{(1)} + dz^{(1)}]$, and one in a patch $d^2\theta^{(2)}$ with redshift in the range $[z^{(2)}, z^{(2)} + dz^{(2)}]$, can be written as

$$P_2 = [\rho^2 p(z^{(1)}) p(z^{(2)}) d^2\theta^{(1)} dz^{(1)} d^2\theta^{(2)} dz^{(2)}] [1 + \xi(r)] . \quad (59)$$

Here $\xi(r)$ is the two-point correlation function of galaxies at mutual (3D) distance r . For distances smaller than $10 h^{-1}$ Mpc, this function can be well approximated as a power law (see Peebles 1993)

$$\xi(r) = \left(\frac{5.4 h^{-1} \text{ Mpc}}{r} \right)^{1.77} , \quad (60)$$

where $h = H_0 / (100 \text{ km s}^{-1} \text{ Mpc}^{-1})$ is the reduced Hubble constant.

We will now evaluate $\text{Cov}(\gamma)$ in the weak lensing limit. In this approximation, the observed ellipticities are related to the unlensed ones by the relation

$$\epsilon_i = \epsilon_i^s - \gamma_{0i}(\boldsymbol{\theta})w(z), \quad (61)$$

and thus the expected covariance on ϵ is given by

$$\text{Cov}_{ij}(\epsilon) = \text{Cov}_{ij}(\epsilon^s) + \text{Var}(w)\gamma_{0i}(\boldsymbol{\theta})\gamma_{0j}(\boldsymbol{\theta}) = c\delta_{ij} + \text{Var}(w)\gamma_{0i}(\boldsymbol{\theta})\gamma_{0j}(\boldsymbol{\theta}). \quad (62)$$

A plot of $\text{Var}(w)$ as a function of the lens redshift for a “typical” redshift distribution $p(z)$ (see Eq. (74) below) is shown in Fig. 13.

A simple estimator of the shear is given by (see Seitz & Schneider 1997)

$$\gamma(\boldsymbol{\theta}) = -\frac{1}{\langle w \rangle_z} \sum_{n=1}^N \epsilon^{(n)} W(\boldsymbol{\theta}, \boldsymbol{\theta}^{(n)}). \quad (63)$$

Since the weight function W is assumed to be normalized following Eq. (46), this is an *unbiased* estimator. In fact (for the procedure of “spatial averaging” see Paper II)

$$\langle \gamma \rangle(\boldsymbol{\theta}) = -\frac{1}{\langle w \rangle_z} \sum_{n=1}^N \langle \epsilon_i^{(n)} \rangle W(\boldsymbol{\theta}, \boldsymbol{\theta}^{(n)}) \simeq \rho \int_{\Omega} W(\boldsymbol{\theta}, \boldsymbol{\theta}') \gamma_0(\boldsymbol{\theta}') d^2\theta'. \quad (64)$$

Thus we recover one simple result already discussed in Paper II: the measured shear is the smoothing of the true shear with the spatial weight function W .

Turning to the covariance of γ , we find

$$\begin{aligned} \text{Cov}_{ij}(\gamma; \boldsymbol{\theta}, \boldsymbol{\theta}') = \frac{1}{\langle w \rangle_z^2} \left\langle \sum_{n,m} [\langle w \rangle_z \gamma_{0i}(\boldsymbol{\theta}^{(n)}) - \epsilon_i^{(n)}] W(\boldsymbol{\theta}, \boldsymbol{\theta}^{(n)}) \times \right. \\ \left. [\langle w \rangle_z \gamma_{0j}(\boldsymbol{\theta}^{(m)}) - \epsilon_j^{(m)}] W(\boldsymbol{\theta}', \boldsymbol{\theta}^{(m)}) \right\rangle. \end{aligned} \quad (65)$$

Inserting here Eq. (61), we find a long expression composed of three types of terms: terms of the form $\langle \epsilon_i^{s(n)} \epsilon_j^{s(m)} \rangle$, terms of the form $\langle \epsilon_i^{s(n)} \rangle$, and terms independent of ϵ^s . Because of the isotropy hypothesis, the first contribution vanishes unless $n = m$ and $i = j$, and the second always vanishes. Thus we finally find

$$\begin{aligned} \text{Cov}_{ij}(\gamma; \boldsymbol{\theta}, \boldsymbol{\theta}') = \frac{1}{\langle w \rangle_z^2} c\delta_{ij} \sum_n W(\boldsymbol{\theta}, \boldsymbol{\theta}^{(n)}) W(\boldsymbol{\theta}', \boldsymbol{\theta}^{(n)}) + \\ \frac{1}{\langle w \rangle_z^2} \left\langle \sum_{n,m} [w(z^{(n)}) - \langle w \rangle_z] \gamma_{0i}(\boldsymbol{\theta}^{(n)}) W(\boldsymbol{\theta}, \boldsymbol{\theta}^{(n)}) \times \right. \\ \left. [w(z^{(m)}) - \langle w \rangle_z] \gamma_{0j}(\boldsymbol{\theta}^{(m)}) W(\boldsymbol{\theta}', \boldsymbol{\theta}^{(m)}) \right\rangle. \end{aligned} \quad (66)$$

This equation is composed of two terms. The first is related to the intrinsic spread of source ellipticities, and in fact it is proportional to $c = \langle |\epsilon^s|^2 \rangle / 2$. The second term (second and third lines in Eq. (66)) is instead related to the spread in redshift of galaxies. In order to obtain a more general expression, we adopt a technique already used in Paper II and average the expression for $\text{Cov}(\gamma)$ over the source positions $\{\boldsymbol{\theta}^{(n)}\}$ and redshifts $\{z^{(n)}\}$. As a result, the first term becomes simply

$$\Gamma_1 = \frac{1}{\langle w \rangle_z^2} c \delta_{ij} \sum_n W(\boldsymbol{\theta}, \boldsymbol{\theta}^{(n)}) W(\boldsymbol{\theta}', \boldsymbol{\theta}^{(n)}) \mapsto \frac{1}{\langle w \rangle_z^2} c \delta_{ij} \rho \int_{\Omega} W(\boldsymbol{\theta}, \boldsymbol{\theta}'') W(\boldsymbol{\theta}', \boldsymbol{\theta}'') d^2 \theta'' . \quad (67)$$

This term has already been studied in detail in Paper II.

The second term of Eq. (66) deserves a more detailed discussion. In order to carry out the average over the source redshifts, we need to split the sum over n and m in two sums, one involving the terms for which $n = m$, and the other involving the terms $n \neq m$. For the first terms we have

$$\begin{aligned} \Gamma_2 &= \frac{1}{\langle w \rangle_z^2} \left\langle \sum_n [w(z^{(n)}) - \langle w \rangle_z]^2 \gamma_{0i}(\boldsymbol{\theta}^{(n)}) \gamma_{0j}(\boldsymbol{\theta}^{(n)}) W(\boldsymbol{\theta}, \boldsymbol{\theta}^{(n)}) W(\boldsymbol{\theta}', \boldsymbol{\theta}^{(n)}) \right\rangle \mapsto \\ &\mapsto \frac{1}{\langle w \rangle_z^2} \rho \text{Var}(w) \int_{\Omega} \gamma_{0i}(\boldsymbol{\theta}'') \gamma_{0j}(\boldsymbol{\theta}'') W(\boldsymbol{\theta}, \boldsymbol{\theta}'') W(\boldsymbol{\theta}', \boldsymbol{\theta}'') d^2 \theta'' . \quad (68) \end{aligned}$$

Note that this term is related to single galaxies, and thus does not involve the correlation function $\xi(r)$. On the other hand, for pairs of galaxies (i.e. if $n \neq m$ in the last term of Eq. (66)) we find a rather complicated expression

$$\begin{aligned} \Gamma_3 &= \frac{1}{\langle w \rangle_z^2} \left\langle \sum_{n \neq m} [w(z^{(n)}) - \langle w \rangle_z] \gamma_{0i}(\boldsymbol{\theta}^{(n)}) W(\boldsymbol{\theta}, \boldsymbol{\theta}^{(n)}) [w(z^{(m)}) - \langle w \rangle_z] \gamma_{0j}(\boldsymbol{\theta}^{(m)}) W(\boldsymbol{\theta}', \boldsymbol{\theta}^{(m)}) \right\rangle \mapsto \\ &\mapsto \frac{1}{\langle w \rangle_z^2} \rho^2 \int_0^\infty p(z'') dz'' \int_{\Omega} d^2 \theta'' \int_0^\infty p(z''') dz''' \int_{\Omega} d^2 \theta''' [w(z'') - \langle w \rangle_z] \gamma_{0i}(\boldsymbol{\theta}'') W(\boldsymbol{\theta}, \boldsymbol{\theta}'') \times \\ &\quad [w(z''') - \langle w \rangle_z] \gamma_{0j}(\boldsymbol{\theta}''') W(\boldsymbol{\theta}', \boldsymbol{\theta}''') \xi(r) . \quad (69) \end{aligned}$$

In this expression r is the distance between two galaxies at redshifts z'' and z''' and angular positions $\boldsymbol{\theta}''$ and $\boldsymbol{\theta}'''$.

The covariance of γ is the sum of the terms in Eqs. (67–69), each of which, as discussed above, arises from a different source of noise. In summary,

- The contribution of Eq. (67) is related to the spread in the intrinsic ellipticities of source galaxies (parameterized by c). It is proportional to $1/\rho$ (see the normalization condition (46)) and has a correlation length proportional to the correlation length of W . Note that this term is proportional to δ_{ij} , so that no correlation between γ_1 and γ_2 arises.

- The contribution of Eq. (68) is related to the spread in redshift of the sources (parameterized by $\text{Var}(w)$). It is proportional to $1/\rho$, has the same correlation length of the previous term, and, in addition, is proportional to γ_0^2 . This term is not diagonal.
- The contribution of Eq. (69) is due to the correlation between galaxies (described by the two-point correlation function $\xi(r)$). It is independent of the density of galaxies (provided $\xi(r)$ does not depend on ρ ; see comments by Peebles 1993 after Eq. (19.39)), has a correlation length somewhat longer than that of the other terms and is proportional to γ_0^2 . This term is not diagonal.

A complete description of the effect of the first term has already been provided in Paper II. Its effect for the detection of a double lens was analyzed in Sect. 5.1.

The order of magnitude of the ratio between the term of Eq. (68) and the one of Eq. (67) can be argued to be

$$\frac{\Gamma_2}{\Gamma_1} \simeq \frac{\text{Var}(w)\gamma_0^2}{c}. \quad (70)$$

Typical values for c are $c \simeq 0.02$, and typical values for $\text{Var}(w)$ can be estimated from Fig. 13. Thus, if we refer to a single lens at redshift $z_d = 0.2$ with a shear of the order of $\gamma \simeq 0.3$, we find $\Gamma_2/\Gamma_1 \simeq 0.2$. Note that, since calculations here are performed in the weak lensing approximation, the shear cannot be much larger than 0.3, and thus the ratio obtained should be taken as an (approximate) upper limit. In any case, the effects of this term will be included in the simulations that will be described in Sect. 6.2.

As to the third term Γ_3 , it is clearly very complex, both in relation to its mathematical structure and to the physical ingredients involved. Therefore, instead of attempting here an order of magnitude estimate for it, we prefer to postpone a complete discussion of its impact to a future paper that will make use of suitable simulations in the cosmological context.

5.3.2. Bias on the reduced shear

Another effect encountered when source galaxies are “placed” at different redshifts is a bias on $\nabla \wedge \mathbf{u}$, which is not bound to vanish any more. This effect could, in principle, be misinterpreted as the signature of a double lens. Do we have to worry about this contribution? Note that if this effect turned out to be significant, it would have an important impact on all single lens mass reconstruction methods, because these are all based on the curl-free character of the shear induced by gravitational lensing.

In order to be more specific about the origin of this effect, we start from some well-known results (Seitz & Schneider 1997; see also Paper III). Let us consider a sample of galaxies with redshift distribution $p(z)$, behind a single cluster at redshift z_d . As the critical density $\Sigma_c(z)$ depends on the source redshift, the lens acts with differential strength on the lensed galaxies (see Sect. 2.1). The cosmological weight function $w(z)$ controls the ray-tracing transformation. In particular, the (redshift dependent) reduced shear takes on the form $g(\boldsymbol{\theta}, z) = w(z)\gamma(\boldsymbol{\theta})/[1 - w(z)\kappa(\boldsymbol{\theta})]$. The fact that $w(z)$ enters the expression of $g(\boldsymbol{\theta}, z)$ nonlinearly complicates the lensing analysis. Note that even though the relevant ray-tracing transformation for a single lens is symmetric (e.g., see Eq. (9) of Paper III), because of the spread in redshift distribution the arguments generally used to identify a curl-free field $\tilde{\mathbf{u}}$ do not hold any more. In fact, if we observe a single lens and just ignore the redshift distribution of the sources, we would naively start by identifying the observed average ellipticity with the reduced shear, using the relation $\langle \epsilon \rangle = -g$. This mistake would lead in general to a quantity $\tilde{\mathbf{u}}$, defined by Eq. (30), with non vanishing curl.

For subcritical lenses Seitz & Schneider (1997) have shown that an accurate, but approximate, lensing analysis can be carried out *as if* all galaxies were at a single redshift, provided the reduced shear $g(\boldsymbol{\theta})$ in Eq. (30) is evaluated from the average ellipticity following the relation $\langle \epsilon \rangle \langle w^2 \rangle_z / \langle w \rangle_z^2 = -g$. Correspondingly, the dimensionless density distribution obtained from the lens reconstruction changes by a factor $\langle w^2 \rangle_z / \langle w \rangle_z$. If the above corrected relation between average ellipticity and reduced shear entering the definition of $\tilde{\mathbf{u}}$ is kept into account, then, in this approximate description, the “spurious curl” (that would be associated with the naive use of $\langle \epsilon \rangle = -g$) is eliminated.

In order to evaluate the magnitude of the effects (described in this subsection) associated with the spread in the distances of the source galaxies, we have carried out simulations that will be described in the next section. Here we summarize the main results. Using a reasonable redshift distribution for the sources, and for a wide range of redshifts z_d of the single deflector, we find an extremely small value of $\nabla \wedge \tilde{\mathbf{u}}$. For example, for a nearly critical single lens at redshift $z_d = 0.3$ the value of the relevant curl is about 50 times smaller than the value associated with the double lens effect addressed in this paper. The nearly critical condition adopted in this example certainly overemphasizes the signal, with respect to the case of weaker lenses, and is unfavorable to the approximation suggested by Seitz & Schneider. Still, if we apply the simple correction factor $\langle w^2 \rangle_z / \langle w \rangle_z^2$ described above, we gain an extra factor of 4. We can thus state that the effect of the redshift distribution discussed in this subsection, in the example considered, is contained to be about 200 times smaller than the effect of double lensing we are interested in. From this we conclude that the simple arguments and derivations provided in the main part of the paper are not affected by the spread in the distances of the source galaxies significantly.

6. Simulations

The main goal of this section is to check the analytical framework developed in the paper and to provide convincing evidence that effects characteristic of double lensing are within reach of the observations. For this reason we follow two types of investigation: a semi-analytical approach (Sect. 6.1), where we test the applicability of our asymptotic analysis, and a study (Sect. 6.2) that may be seen as a numerical observation, where we simulate the distortions of a set of source galaxies in a given field under realistic conditions (see below) and we perform the statistical lensing analysis on the observed ellipticities. For simplicity, the simulations are carried out under the assumption that no clustering is present in the source population (Eq. (59) with $\xi(r) = 0$).

6.1. Check of the analytical framework

A first test is based on the following steps of a semi-analytical approach:

- The population of source galaxies is taken to be at a single redshift ($z_s = 2.0$).
- A simple model of a double lens is chosen. For simplicity, two centrally-symmetric projected mass distributions are used, within a favorable geometric configuration (see Sect. 4.1).
- The two clusters are taken to be located at redshift $z^{(1)} = 0.1$ and $z^{(2)} = 0.4$. Since the source population and the double lens we have in mind have such large distances, the values of the cosmological parameters Ω and Ω_Λ need to be specified. In the following we refer to the case $\Omega = 0.3$, $\Omega_\Lambda = 0.7$; moreover, we adopt $H_0 = 65 \text{ km s}^{-1} \text{ Mpc}^{-1}$.
- The two functions $\beta^{(1)}(\boldsymbol{\theta})$ and $\beta^{(2)}(\boldsymbol{\theta})$ are calculated. Thus the ray-tracing function $\theta^s(\boldsymbol{\theta})$ is derived (see Eq. (8)).
- The Jacobian matrix $A_0(\boldsymbol{\theta})$ is calculated from the map $\theta^s(\boldsymbol{\theta})$. This allows us to calculate the various quantities defined in Eqs. (18–21). In the following, these are taken to hold as definitions also for strong lenses.
- The “effective” Jacobian matrix $A_s(\boldsymbol{\theta})$ is obtained from $A_0(\boldsymbol{\theta})$ using Eq. (15).
- From $A_s(\boldsymbol{\theta})$, the reduced shear $g(\boldsymbol{\theta})$ and the field $\tilde{\mathbf{u}}(\boldsymbol{\theta})$ are calculated.
- The divergence and the curl of $\tilde{\mathbf{u}}$ are compared with the Laplacians of $\ln(\sigma)$ and τ (Eqs. (31) and (32)).

Note that, by following this procedure, we are considering the “effective” Jacobian matrix A_s *without errors*. We do so, because errors on A_s are discussed separately (see next Subsection 6.2, and Paper I and II) and because we are focusing here mostly on a test of the adequacy of Eqs. (31) and (32). Let us now describe some of the steps in further detail.

The two clusters, taken to be located at redshift $z^{(1)} = 0.1$ and $z^{(2)} = 0.4$ (so that the value of the parameter Δ defined in Eq. (5) is $\Delta \simeq 0.794$ in the assumed cosmological model), have been modeled using the following profiles (close to isothermal profiles) for the projected density (see Schneider, Ehlers, & Falco 1992):

$$\kappa(\boldsymbol{\theta}) = \frac{[1 + (\theta/\theta_c)^2/2]\kappa_c}{[1 + (\theta/\theta_c)^2]^{3/2}}, \quad (71)$$

with $\theta = \|\boldsymbol{\theta}\|$. Here $\kappa_c = \kappa(\mathbf{0})$ is the maximum value of the projected density, and θ_c is a length scale (core radius). The deflection $\beta(\boldsymbol{\theta})$ for such profiles takes a particularly simple form:

$$\beta(\boldsymbol{\theta}) = \frac{\kappa_c}{\sqrt{1 + (\theta/\theta_c)^2}} \boldsymbol{\theta}. \quad (72)$$

The intrinsic *physical* parameters of the two clusters, i.e. the core radius in Mpc and central density in kg m^{-2} ($1 \text{ kg m}^{-2} \simeq 478 M_\odot \text{ pc}^{-2}$) have been assumed to be equal. For simplicity, the first cluster is centered at $\boldsymbol{\theta} = (5', 3' 30'')$ and the second cluster at $\boldsymbol{\theta} = (5', 6' 30'')$. In addition, we have considered two cases: a case of “weak” lenses, for which the second order expansion considered in Sect. 3 is expected to provide accurate results, and a case of “strong” lenses, with “joint mass density” $1 - \sigma$ too high in relation to the asymptotic expansion. For the strong case the mass associated within our field of $10' \times 10'$ for the far cluster is $M \simeq 3.14 \times 10^{15} M_\odot$. The latter case will show that, at least qualitatively, the analysis developed in this paper is applicable even to relatively strong lenses. The cluster parameters adopted for the tests presented here are summarized in Table 1.

In Figs. 2 and 3 we display the combined luminosity and dimensionless density distributions.

The second step has been the calculation of the ray-tracing function $\boldsymbol{\theta}^s(\boldsymbol{\theta})$. This function has been calculated on a grid of 100×100 points, representing a square with a side of $10'$.

Table 1: The parameters used for the simulations.

component		redshift	density		core radius	
		z	κ_c	$\kappa_c \Sigma_c$ (kg m $^{-2}$)	θ_c (angle)	r_c (Mpc)
weak	cl 1	0.1	0.054	0.5	2' 31''	0.3
	#2	0.4	0.120	0.5	0' 52''	0.3
strong	cl 2	0.1	0.401	3.7	2' 31''	0.3
	#2	0.4	0.891	3.7	0' 52''	0.3

The Jacobian matrix has been calculated on the same grid using the approximate derivatives determined from the differences of θ^s in neighboring points.

The plot of the semi-trace σ of A_0 (see Eq. (19)) presents some interesting features. We first note that for weak lenses $\sigma = 1 - \kappa^{(1)} - \kappa^{(2)}$. However, when the lens is strong, a curious effect is noted (cfr. Fig. 4): the maximum corresponding to the mass distribution of the second cluster is significantly smoothed and lowered. This has to do with the coupling of the two deflectors. The effect can be broadly described as a *magnification* of the mass distribution of the second deflector because of the lensing effect of the first cluster. In fact, while the value of $\kappa^{(1)} + \kappa^{(2)}$ exceeds unity (see Fig. 3), the double lens remains sub-critical with $1 - \sigma$ below unity.

Proceeding along the list of steps indicated above, we have calculated the reduced shear $g(\theta)$ and the field $\tilde{\mathbf{u}}(\theta)$. At the end of the process, the two quantities $\nabla \cdot \tilde{\mathbf{u}}$ and $\nabla \wedge \tilde{\mathbf{u}}$ are available on a 100×100 grid. Note that all differentiations have been performed using a 3-point, Lagrangian interpolation.

The results of our tests for the weak case are summarized in Figs. 5–7. Within the numerical errors, we find that Eqs. (31) and (32) are verified. Of course, since in this case the magnitude of the effect is very small (the maximum value of τ is approximately 2×10^{-4}), we should not expect that double lensing of this type could be actually detected. In passing we note that the order of magnitude for the various quantities shown in the figures is consistent with this value of τ .

The tests for the strong case (see Figs. 8–10) are rather surprising. In fact, Fig. 8 shows that Eq. (31) holds approximately also in this case. However, Eq. (32) turns out to be inadequate, as shown by Fig. 9. This behavior reflects the fact that the lens configuration here has a rather high value of $1 - \sigma$ (its maximum is about 0.928), and a small value of τ (maximum about 0.01). A heuristic way to correct Eq. (32) is the following:

$$\nabla \wedge \tilde{\mathbf{u}} = \nabla \cdot \left(\frac{\nabla \tau}{\sigma} \right). \quad (73)$$

The use of σ in the denominator of the previous equation is suggested by analogy with Eq. (31), where $\nabla(\ln \sigma) = (\nabla \sigma)/\sigma$ is used. Moreover, we note that, to second order, Eq. (73) is identical to Eq. (32). The new equation turns out to be a better approximation than Eq. (32), especially for regimes away from the strong and the weak limiting cases considered above; in such intermediate cases Eq. (73) performs better, typically by a factor of 2.

Finally, we have considered the problem of the dark cluster (see Sect. 4.4). In this case the simplified simulations in the semi-analytical approach described above have been performed with the aim of demonstrating how the redshift of a dark cluster can be determined when the redshift and the mass distribution of the luminous cluster are known. In order to find the unknown redshift we have minimized S , the integral of the square of the left hand side of Eq. (43) or of Eq. (44),

depending on whether the dark cluster is considered to be closer to us than the luminous cluster or not. Simulations have been performed using the parameters of the strong lens configuration, by taking either the first or the second cluster as the dark cluster. Figure 11 shows S for the case where the dark cluster is in the front, while Fig. 12 shows the same quantity for the case where the dark cluster is behind. Note that S has a minimum (near or equal to 0) for the true redshift of the dark cluster. Note also that the second minimum of S occurs where the condition $\Delta = 0$ is met: in this case the quantities $\zeta^{(1)}$, $\zeta^{(2)}$, and ζ^s all reduce to θ . We should stress that if a dark cluster is detected from a double lens signature, as described in this paper, and if the key characteristics of the bright cluster are known from independent diagnostics, then *the reconstruction method developed here leads to the full determination of both the distance and the mass distribution of the invisible cluster.*

6.2. More realistic simulations

In order to ascertain the relevance of our analysis with respect to present and future observations, we have performed a set of simulations described in the following steps:

- We generate N source galaxies. Each galaxy is described by its location in the sky, its redshift, and its source ellipticity. Locations are chosen following a uniform distribution on the observed locations θ (thus neglecting the magnification effect). The redshift of source galaxies has been drawn from a gamma distribution used also by other authors (e.g., Brainerd et al. 1996)

$$p(z) = \frac{z^2}{2z_0^3} \exp[-(z/z_0)] , \quad (74)$$

with $z_0 = 1/3$ (other values of z_0 have also been tested). Finally, ellipticities ϵ^s are taken from a truncated Gaussian distribution (see Eq. (32) of Paper III) characterized by $c = 0.02$. This value is probably unrealistically large; it is adopted in order to test our framework under relatively unfavorable conditions.

- As a model for the double lens we use the “strong” double lens model introduced in the previous subsection, within the same field of view of $10' \times 10'$.
- Source ellipticities ϵ^s are transformed into observed ellipticities ϵ using the true asymmetric Jacobian matrix associated with the lens. Note that the redshift of each galaxy has been taken into account when performing this transformation.

- The statistical lensing reconstruction procedure is applied to the observed ellipticities. The reduced shear map $g(\boldsymbol{\theta})$ is derived by averaging observed ellipticities of nearby galaxies, from the relation $\langle \epsilon \rangle = -g$ properly corrected for the redshift distribution.
- From the shear map we calculate the other relevant quantities: the vector field $\tilde{\mathbf{u}}(\boldsymbol{\theta})$, its divergence, and its curl.
- We then look for significant peaks in the curl map, which would reveal the double nature of the lens.

Several simulations have been performed with different source galaxy densities. The results obtained are very encouraging, since a significant signal in the the curl of $\tilde{\mathbf{u}}$ is already detected with a galaxy density of $100 \text{ gal arcmin}^{-2}$. Such relatively high density has already been reached by current observations. For example, new observations with the Very Large Telescope of the cluster MS1008.1–1224 come close to it (Lombardi et al. 2000, Athreya et al. 2000; see also Hoekstra et al. 2000 for observations of MS1054 with the HST).

Figure 14 shows a typical result obtained in our simulations. The figure shows the density plot of the observed $\nabla \wedge \tilde{\mathbf{u}}$ and, superimposed, the contour plot of $\nabla \wedge \tilde{\mathbf{u}}_0$, i.e. the true quantity that we should measure in the limit of infinite galaxy density. For both plots we have used the same smoothing spatial weight function, a Gaussian of width $\sigma_W = 30''$ (see Sect. 5.2). We thus conclude that, given the conditions adopted in our simulations, the characteristic signature of double lensing should be within reach of current observations.

Finally, in order to test the reliability of the detection, we have performed analogous simulations using a single cluster. In this case, as explained above, we expect a (nearly) vanishing $\nabla \wedge \tilde{\mathbf{u}}$, especially after the correction for the spread of background sources is applied (see Sect. 5.3.2). Figure 15 shows a map of this quantity (with the correction applied) in the case of a single lens at redshift 0.1 (the parameters of this lens are the same as those of the first lens considered in the double configuration). Note that the noise observed is well below the signal shown in Figure 14.

7. Conclusions

In this paper we have generalized the statistical analysis at the basis of mass reconstructions of weak gravitational lenses from the standard case of single lenses to the case of double lenses. From one point of view, this study leads to practical tools to deal with “errors” that might occur when the standard single lens analyses are applied to the not infrequent cases where two massive clusters happen to be partially aligned along the line of sight. In reality, our study of double lenses,

based on the analytical framework mentioned in the first item below then checked and extended by means of simulations, has opened the way to a number of interesting results. This is a list of the main points made in our paper:

1. A consistent analytical framework has been constructed where the contribution of the small asymmetry in the Jacobian matrix induced by double lensing is retained to two orders in the weak lensing asymptotic expansion.
2. Given the known properties of the distribution of (bright) clusters of galaxies, we have shown that a few configurations are likely to be present in the sky, for which the small effects characteristic of double lensing may already be within detection limits.
3. As a separate astrophysical application, we have demonstrated that, if the characteristic signature of double lensing appears in an observed configuration where a single bright cluster exists, with properties well constrained by independent diagnostics, the location and the mass distribution of the dark cluster, if present and responsible for the effect, can in principle be reconstructed unambiguously.
4. We have checked that the redshift distribution of the source galaxies should not confuse the signature of double lensing.
5. An examination of the relevant contributions to the noise of the shear measurements has brought up a limitation of weak lensing analyses related to the clustering of source galaxies. In particular, weak lensing studies of single clusters are found to be characterized by a lower limit for the expected noise, regardless of the depth of the images and of the density of source galaxies. A firm quantitative estimate of this surprising effect will be provided in a separate article.

This work was partially supported by MURST of Italy. We thank Peter Schneider for several stimulating discussions that have helped us improve this paper significantly.

A. Second order weak lensing analysis

In this Appendix we derive Eqs. (31) and (32).

We start from the definition of $\tilde{\mathbf{u}}$, which, to second order, is

$$\tilde{\mathbf{u}} = \begin{pmatrix} 2 - \sigma + \gamma_1 & \gamma_2 \\ \gamma_2 & 2 - \sigma - \gamma_1 \end{pmatrix} \begin{pmatrix} \gamma_{1,1} + \gamma_{2,2} \\ \gamma_{2,1} - \gamma_{1,2} \end{pmatrix} - \begin{pmatrix} \sigma_{,1} & \sigma_{,2} \\ \sigma_{,2} & -\sigma_{,1} \end{pmatrix} \begin{pmatrix} \gamma_1 \\ \gamma_2 \end{pmatrix}. \quad (\text{A1})$$

We recall that $\sigma = 1 + \mathcal{O}(\epsilon)$. By inserting Eqs. (19–21) here, rather long expressions are found:

$$\tilde{u}_1 = \frac{1}{4} \left[4\nabla^2 \theta_1^s - \theta_{1,11}^s \nabla \cdot \boldsymbol{\theta}^s - 2\theta_{1,22}^s \theta_{2,2}^s + \theta_{2,12}^s (\theta_{2,2}^s - \theta_{1,1}^s) + (\theta_{1,2}^s + \theta_{2,1}^s) \nabla \wedge \boldsymbol{\theta}_{,1}^s \right], \quad (\text{A2})$$

$$\tilde{u}_2 = \frac{1}{4} \left[4\nabla^2 \theta_2^s - \theta_{2,22}^s \nabla \cdot \boldsymbol{\theta}^s - 2\theta_{2,11}^s \theta_{1,1}^s - \theta_{1,12}^s (\theta_{2,2}^s - \theta_{1,1}^s) - (\theta_{1,2}^s + \theta_{2,1}^s) \nabla \wedge \boldsymbol{\theta}_{,2}^s \right]. \quad (\text{A3})$$

From these expressions we can calculate the divergence and the curl of $\tilde{\mathbf{u}}$. The expressions obtained by a straightforward application of the definitions contain also terms of order ϵ^3 or higher, which are to be discarded.

Let us start from the curl of $\tilde{\mathbf{u}}$. From the previous equations, after some manipulations, we obtain

$$\begin{aligned} \nabla \wedge \tilde{\mathbf{u}} = & \nabla^2 (\nabla \wedge \boldsymbol{\theta}^s) - \frac{1}{2} \left[\theta_{1,1}^s \nabla \wedge \boldsymbol{\theta}_{,11}^s + \theta_{2,2}^s \nabla \wedge \boldsymbol{\theta}_{,22}^s + \right. \\ & (\theta_{1,2}^s + \theta_{2,1}^s) \nabla \wedge \boldsymbol{\theta}_{,12}^s + \\ & \theta_{1,11}^s \nabla \wedge \boldsymbol{\theta}_{,1}^s + \theta_{2,22}^s \nabla \wedge \boldsymbol{\theta}_{,2}^s + \\ & \left. \theta_{1,12}^s \theta_{1,22}^s - \theta_{2,11}^s \theta_{2,12}^s \right]. \end{aligned} \quad (\text{A4})$$

The terms in this expression are organized by rows. Recalling that $\nabla \wedge \boldsymbol{\theta}^s = 2\tau \sim \epsilon^2$, we recognize that the terms in the second and third lines are of order ϵ^3 , and thus should be dropped. A simple analysis also shows that the two terms in the last line cancel out. Finally, as to the first line, we note that $\theta_{1,1}^s$ and $\theta_{2,2}^s$ are of the form $1 + \mathcal{O}(\epsilon)$. Thus at the end we obtain

$$\nabla \wedge \tilde{\mathbf{u}} \simeq \frac{1}{2} \nabla^2 (\nabla \wedge \boldsymbol{\theta}^s), \quad (\text{A5})$$

that is Eq. (32).

Let us now turn to the divergence of $\tilde{\mathbf{u}}$. From Eqs. (A2) and (A3), a rather long calculation

gives

$$\begin{aligned}
\nabla \cdot \tilde{\mathbf{u}} = & \nabla^2 (\nabla \cdot \boldsymbol{\theta}^s) + \\
& \frac{1}{4} \left[\nabla \cdot \boldsymbol{\theta}^s (\theta_{1,122}^s - \theta_{1,111}^s + \theta_{2,112}^s - \theta_{2,222}^s) - \right. \\
& 4\theta_{1,1}^s \theta_{2,112}^s - 4\theta_{2,2}^s \theta_{1,122}^s - \\
& \nabla^2 \theta_1^s (\theta_{1,11}^s - \theta_{1,22}^s + 2\theta_{2,12}^s) + \\
& \nabla^2 \theta_2^s (\theta_{2,11}^s - \theta_{2,22}^s - 2\theta_{1,12}^s) + \\
& \left. (\theta_{1,2}^s + \theta_{2,1}^s) (\nabla \wedge \boldsymbol{\theta}_{,11}^s - \nabla \wedge \boldsymbol{\theta}_{,22}^s) \right] .
\end{aligned} \tag{A6}$$

The first line of this expression needs no special explanations, since we recall that $\nabla \cdot \boldsymbol{\theta}^s = 2\sigma$. The sum of the terms in the second and third lines can be shown to be equal (dropping terms of order ϵ^3 or higher) to $-4\sigma \nabla^2 \sigma$. By replacing $2\theta_{2,12}^s$ by $2\theta_{1,22}^s$ and $2\theta_{1,12}^s$ by $2\theta_{2,11}^s$ (which is allowed to second order), the terms in parentheses in the fourth and fifth lines become respectively $\nabla^2 \theta_1^s$ and $\nabla^2 \theta_2^s$. Finally, the last line can be discarded, because it contains two terms of order ϵ^3 . In conclusion, we obtain

$$\nabla \cdot \tilde{\mathbf{u}} \simeq 2\nabla^2 \sigma - \sigma \nabla^2 \sigma - \frac{1}{4} \|\nabla^2 \boldsymbol{\theta}^s\|^2 . \tag{A7}$$

This expression can be replaced by $\nabla^2(\ln \sigma)$. In fact, to second order we have

$$\nabla^2(\ln \sigma) = (2 - \sigma) \nabla^2 \sigma - \|\nabla \sigma\|^2 . \tag{A8}$$

We now apply the vector identity $\nabla(\nabla \cdot \mathbf{A}) = \nabla^2 \mathbf{A} - \nabla \wedge \nabla \wedge \mathbf{A}$ (valid for any vector field \mathbf{A}) to the last term of Eq. (A8):

$$\begin{aligned}
\|\nabla(\nabla \cdot \boldsymbol{\theta}^s)\|^2 = & \|\nabla^2 \boldsymbol{\theta}^s\|^2 - 2(\nabla^2 \boldsymbol{\theta}^s) \cdot (\nabla \wedge \nabla \wedge \boldsymbol{\theta}^s) + \\
& \|\nabla \wedge \nabla \wedge \boldsymbol{\theta}^s\|^2 = \|\nabla^2 \boldsymbol{\theta}^s\|^2 ,
\end{aligned} \tag{A9}$$

where the last equality holds because $\nabla \wedge \boldsymbol{\theta}^s = 2\tau$ is of order ϵ^2 . Thus finally we can rewrite Eq. (A8) as

$$\nabla^2(\ln \sigma) = (2 - \sigma) \nabla^2 \sigma - \frac{1}{4} \|\nabla^2 \boldsymbol{\theta}^s\|^2 . \tag{A10}$$

Comparing this expression with Eq. (A7) we obtain the desired relation (31).

REFERENCES

Athreya, R., Mellier, Y., Van Waerbeke, L., Fort, B., Pello, R., Dantel-Fort M. 2000, submitted (astro-ph/9909518)

- Bartelmann, M., Narayan, R., Seitz, S., & Schneider, P. 1996, ApJ 464, L115
- Borgani, S., Rosati, P., Tozzi, P., & Norman, C. 1999, ApJ 517, 40
- Brainerd, T., Blandford, R., Smail, I. 1996, ApJ 466, 623
- Crawford, C. S., Fabian, A. C., Rees, M. J. 1986, Nature 323, 514
- Girardi, M., Borgani, S., Giuricin, G., Mardirossian, F., & Mezzetti, M. 1998, ApJ 506, 45
- Hoekstra, H., Franx, M., Kuijken, K. 2000, ApJ, 532, 88
- Kaiser, N. 1995, ApJ 439, L1
- Kaiser, N. 1998, ApJ 498, 26
- Kaiser, N., Jaffe, A. 1997, ApJ 484, 545
- Kaiser, N., & Squires, G. 1993, ApJ 404, 441
- Kaiser, N., Squires, G., & Broadhurst, T. 1995, ApJ 449, 460
- Lombardi, M. 2000, PhD Thesis, Scuola Normale Superiore, Pisa
- Lombardi, M., & Bertin, G. 1998a, A&A 330, 791 (Paper I)
- Lombardi, M., & Bertin, G. 1998b, A&A 335, 1 (Paper II)
- Lombardi, M., & Bertin, G. 1999, A&A 342, 337 (Paper III)
- Lombardi, M., Rosati, P., Nonino, M., Girardi, M., Borgani, S., Squires, G. 2000, submitted
- Luppino, G. A., & Kaiser, N. 1997, ApJ 475, 20
- Molinari, E., Buzzoni, A., & Chincarini, G. 1996, A&AS 119, 391
- Peebles, P.J.E. 1980, The Large Scale Structure of the Universe (Princeton University Press: Princeton)
- Peebles, P.J.E. 1993, Principles of Physical Cosmology (Princeton University Press: Princeton)
- Schneider, P., Ehlers J., & Falco, E. E. 1992, Gravitational Lenses (Springer-Verlag: Berlin)
- Schneider, P., Seitz C. 1995, A&A 294, 411
- Seitz, C., & Schneider, P. 1997, A&A 318, 687

Seitz, S., & Schneider, P. 1992, A&A 265, 1

Seitz, S., & Schneider, P. 1994, A&A 287, 349

Taylor, A. N., Dye, S., Broadhurst, T. J., Benitez, N., & Van Kampen, E. 1998 ApJ, 501, 539

van Waerbeke, L., Bernardeau, F. & Mellier, Y. 1999, A&A 342, 15

Wang, Q. D., & Ulmer, M. P. 1997, MNRAS 292, 920

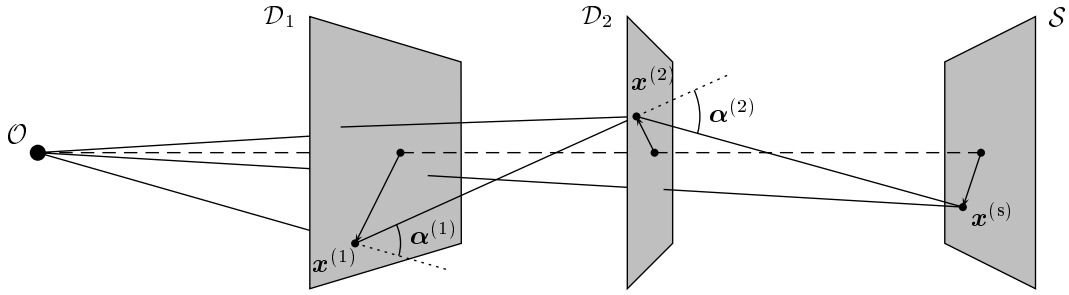


Fig. 1.— The geometrical configuration of a double lens system: the observer \mathcal{O} , the two deflector planes \mathcal{D}_1 and \mathcal{D}_2 , and the source plane \mathcal{S} .

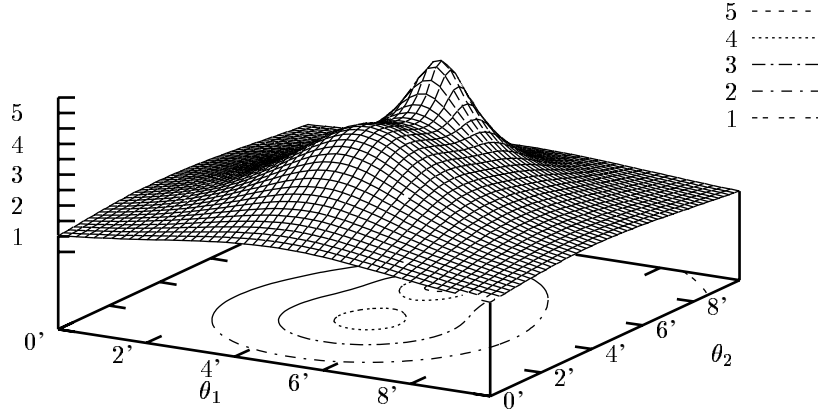


Fig. 2.— This plot shows the light distribution, in arbitrary units, that would be observed if the two clusters had equal and constant mass-to-light ratio. Note that the peak corresponding to the center of the far cluster is slightly higher, because of the contribution by the near cluster, which appears to be more diffuse.

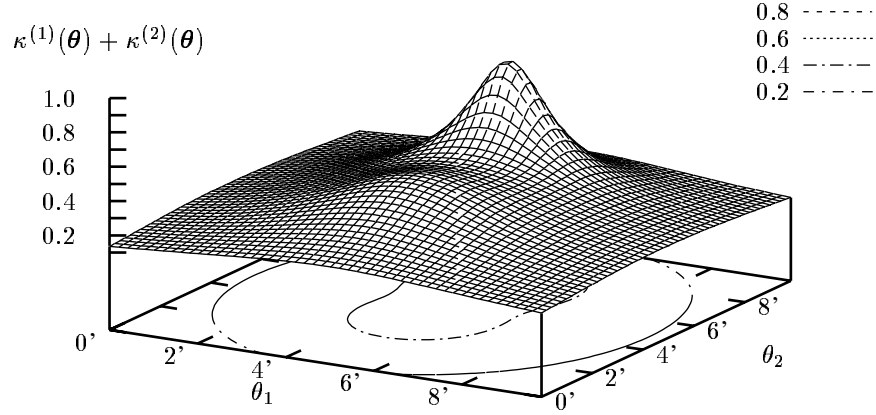


Fig. 3.— The sum of the dimensionless mass distributions $\kappa^{(1)}(\boldsymbol{\theta})$ and $\kappa^{(2)}(\boldsymbol{\theta})$ for the strong case. Note that, although the two clusters are physically identical, the near cluster appears to be significantly weaker and more diffuse. The maximum value reached by the combined dimensionless mass distribution is $\kappa^{(1)} + \kappa^{(2)} \simeq 1.072$. However, the lens is still sub-critical (the maximum value for $1 - \sigma$ is about 0.928).

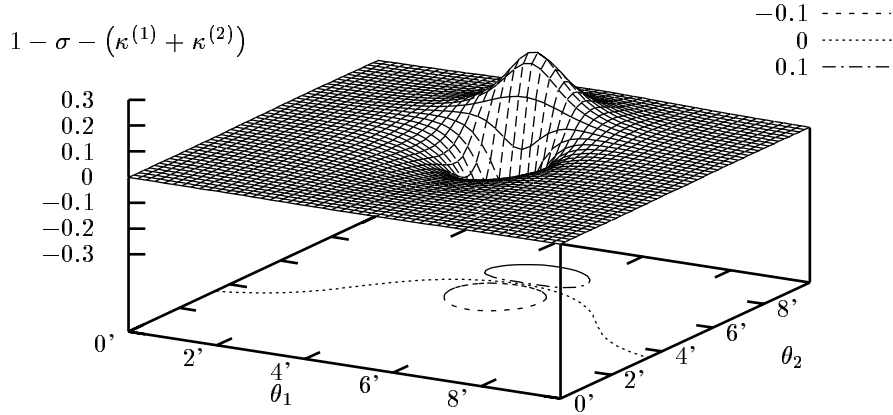


Fig. 4.— The quantity $1 - \sigma - (\kappa^{(1)} + \kappa^{(2)})$ plotted here for the strong case shows a “hole” and a “peak” which can be understood in terms of the lens effect of the near cluster on the “effective” mass of the second cluster. The quantity shown here vanishes only in the weak lensing limit.

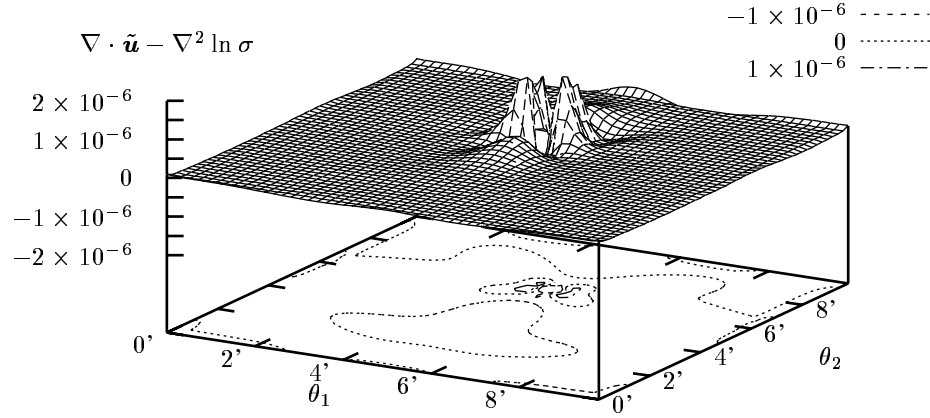


Fig. 5.— The difference $\nabla \cdot \tilde{\mathbf{u}} - \nabla^2 \ln \sigma$ on the θ -plane for the weak case. As described in the text, to second order this quantity is expected to vanish (Eq. (31)). For comparison, we note that the maximum value of $|\nabla \cdot \tilde{\mathbf{u}}|$ is about 0.00647.

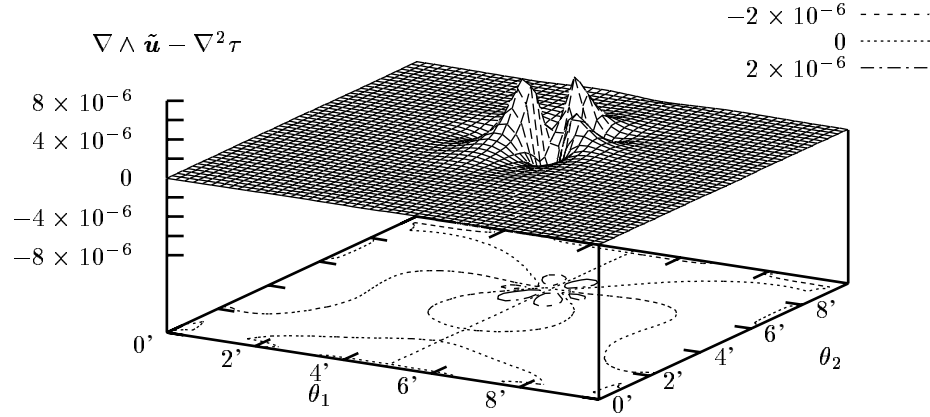


Fig. 6.— The difference $\nabla \wedge \tilde{\mathbf{u}} - \nabla^2 \tau$ on the θ -plane for the weak case. As described in the text, to second order this quantity is expected to vanish (Eq. (32)). The maximum value of $|\nabla \wedge \tilde{\mathbf{u}}|$ is about 3.37×10^{-5} .

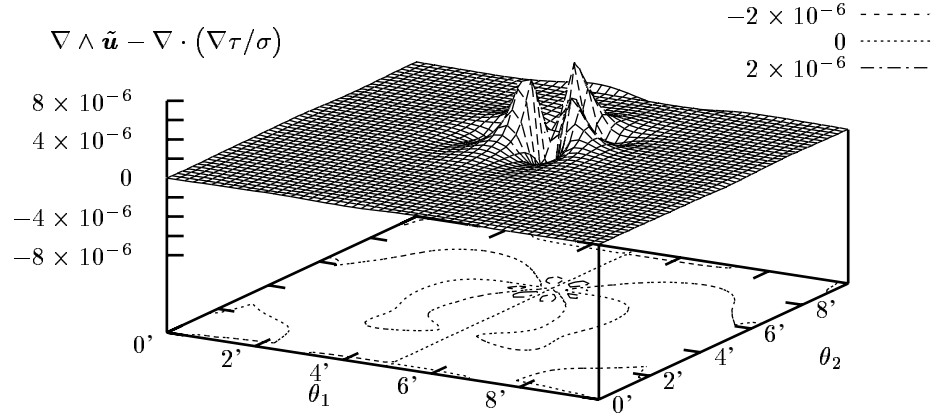


Fig. 7.— The difference $\nabla \wedge \tilde{\mathbf{u}} - \nabla \cdot (\nabla \tau / \sigma)$ on the θ -plane for the weak case. To second order, $\nabla \cdot (\nabla \tau / \sigma) = \nabla^2 \tau$, and in fact the plot shown here is very similar to that of Fig. 6.

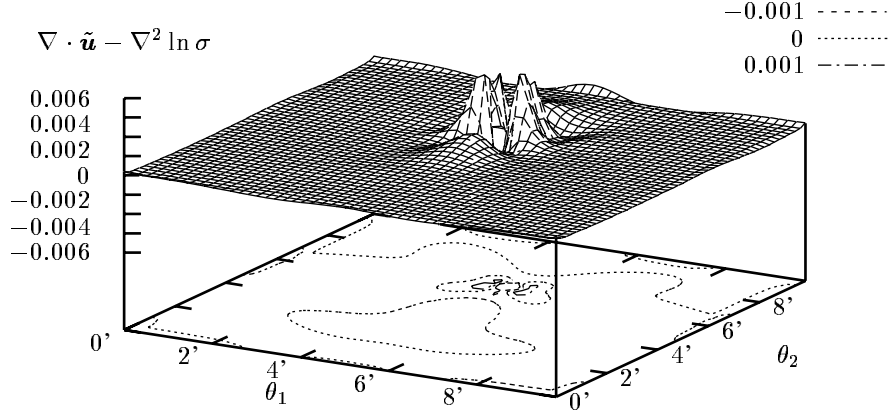


Fig. 8.— As in Fig. 5, but for the strong case. Note that the difference shown remains small. For comparison, the maximum value of $|\nabla \cdot \tilde{\mathbf{u}}|$ is about 0.331.

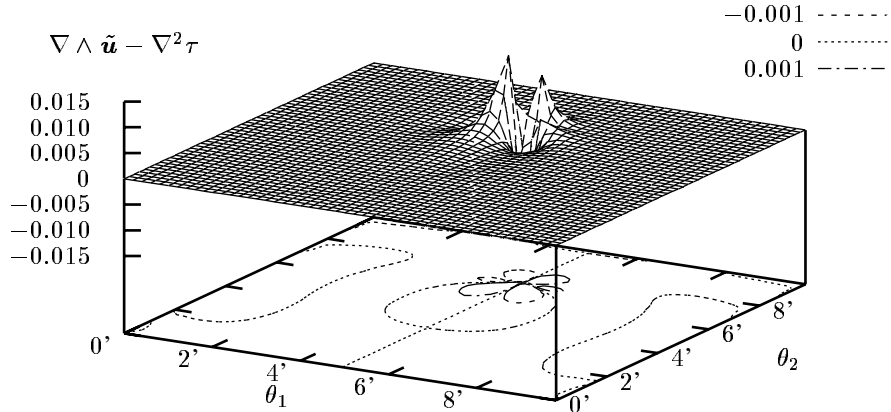


Fig. 9.— As in Fig. 6, but for the strong case. The maximum value of $|\nabla \wedge \tilde{\mathbf{u}}|$ is about 0.0167.

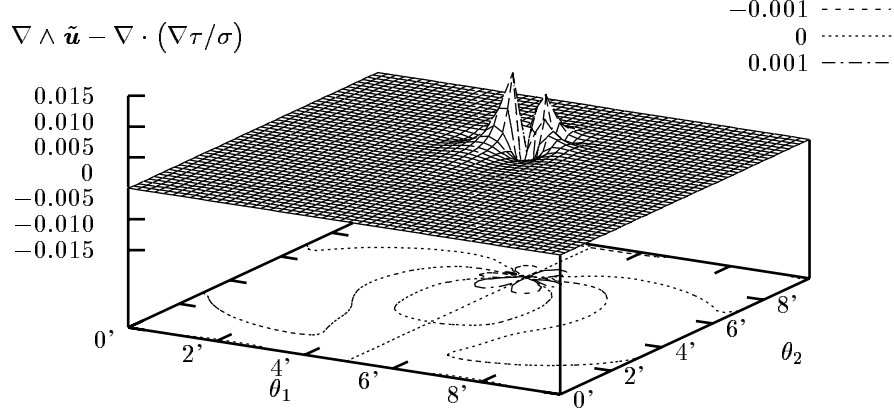


Fig. 10.— As in Fig. 7, but for the strong case.

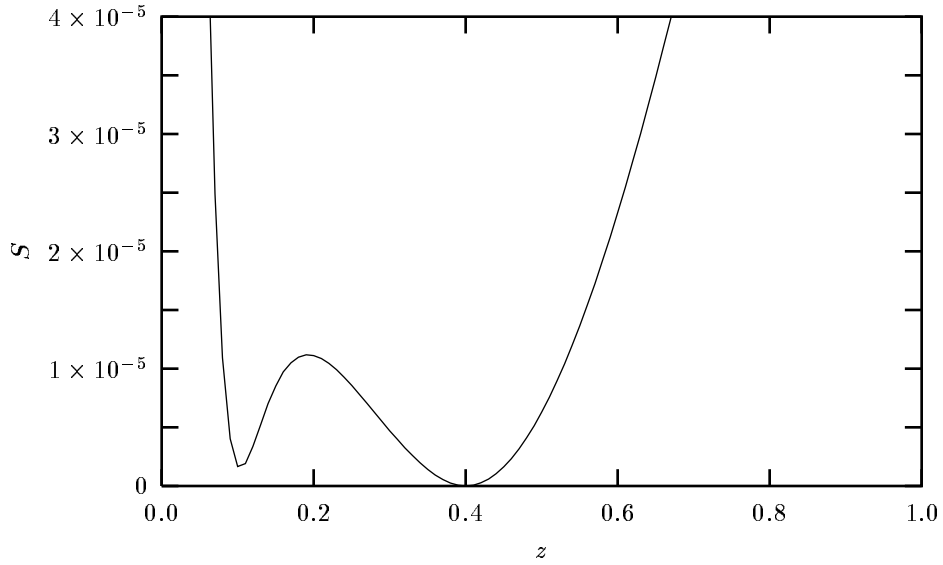


Fig. 11.— The detection of a dark cluster at redshift $z = 0.1$. The value of the integral S (see text for definition) is shown as a function of the redshift z of the dark cluster. Note that S does not exactly vanish at $z = 0.1$ because of discretization errors. The luminous cluster is at redshift $z_{\text{lum}} = 0.4$.

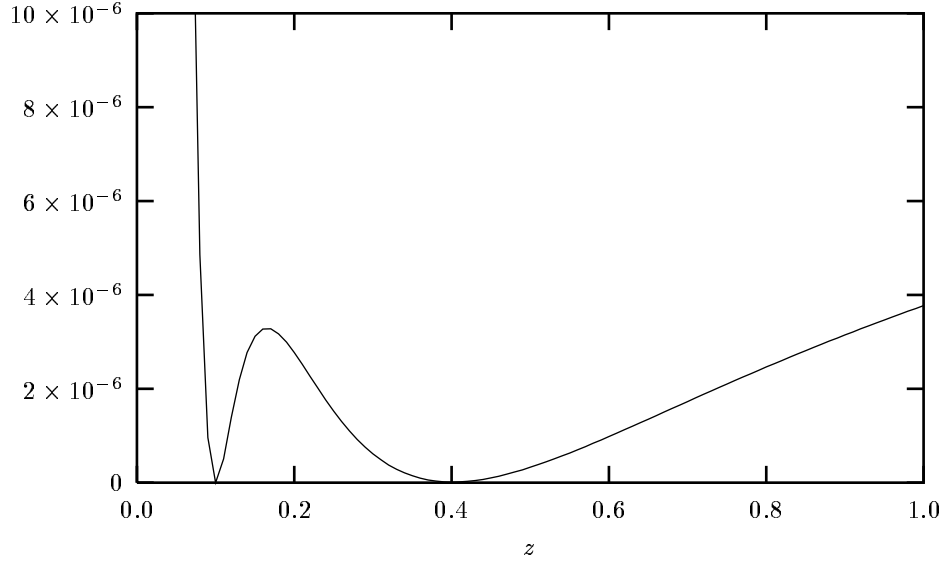


Fig. 12.— As for Fig. 11, but with the luminous and the dark cluster locations swapped. The function S has been computed on sampled redshifts, and for this reason the minimum at $z = 0.1$ appears to be somewhat jagged.

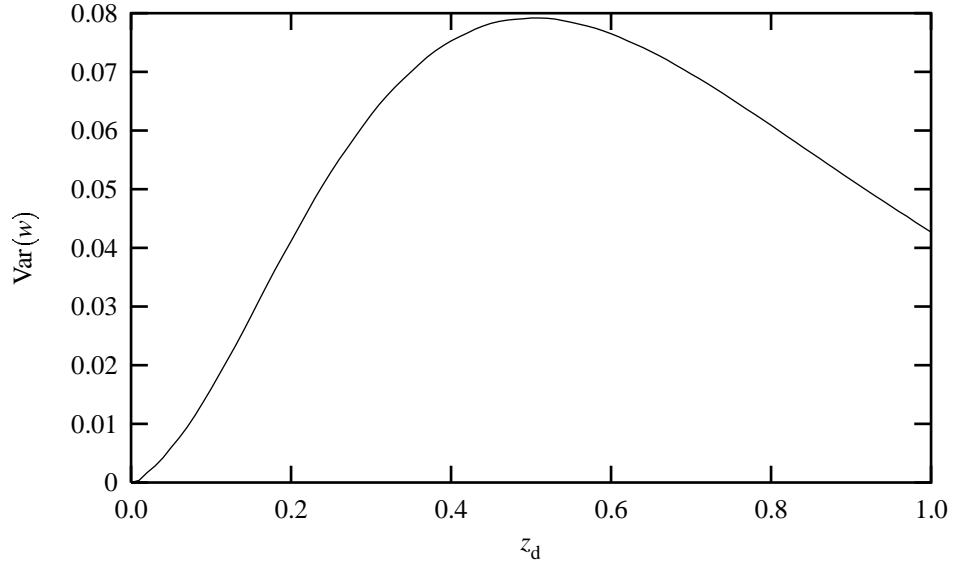


Fig. 13.— Variance of w as a function of the lens redshift z_d ($\Omega_0 = 0.3, \Omega_\Lambda = 0.7$). The assumed source probability distribution is given by Eq. (74).

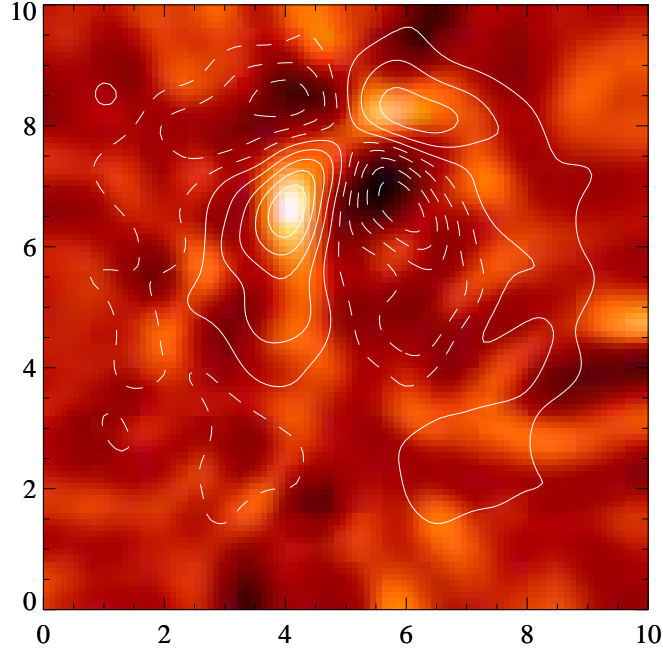


Fig. 14.— Density plot of $\nabla \wedge \tilde{\mathbf{u}}$ for the “strong” double lens. This plot has been obtained by simulating the observation of galaxies in a field of $10' \times 10'$. The adopted galaxy density is $100 \text{ gal arcmin}^{-2}$. The superimposed contour plot describes the quantity $\nabla \wedge \tilde{\mathbf{u}}_0$, after suitable smoothing. Contours are at levels $[\pm 3, \pm 9, \pm 15, \pm 21, \pm 27] \times 10^{-5}$ (positive contours are solid, negative ones are dashed). Because of a different choice for the unit of length, the contour levels of $\nabla \wedge \tilde{\mathbf{u}}$ shown here should not be compared directly with those plotted in Fig. 9. The plane represented in the figure is precisely the (θ_1, θ_2) plane as drawn in Fig. 3.

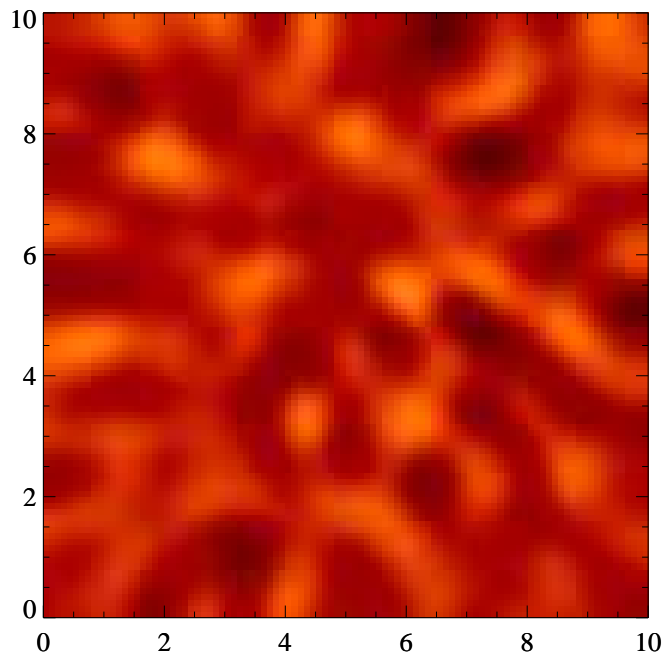


Fig. 15.— Same as Fig. 14 but for a single lens at redshift $z = 0.1$. Equal gray levels in the two pictures correspond to equal values for $\nabla \wedge \tilde{u}$. A comparison of the signal in the previous figure with the noise observed here provides an estimate of the detection significance of a double lens. Note that most of the noise in this map is due to the finite ellipticity of source galaxies and, to a smaller extent, to the spread in redshift of galaxies.